Journal: Engineering Structures

Damage detection in railway bridges using traffic-induced dynamic responses

Andreia Meixedo[1], João Santos[2], Diogo Ribeiro[3], Rui Calçada[4], Michael Todd[5]

ABSTRACT

This paper aims at detecting damage in railway bridges based on traffic-induced dynamic responses. To achieve this goal, an unsupervised automatic data-driven methodology is proposed, consisting of a combination of time series analysis methods and multivariate statistical techniques. Damage-sensitive features of train-induced responses are extracted and allow taking advantage, not only of the repeatability of the loading, but also, and more importantly, of its great magnitude, thus enhancing the sensitivity to small-magnitude structural changes.

The efficiency of the proposed methodology is validated in a long-span steel-concrete composite bowstring-arch railway bridge with a permanent structural monitoring system installed. An experimentally validated finite element model was used, along with experimental values of temperature, noise, and train loadings and speeds, to realistically simulate baseline and damage scenarios.

The proposed methodology proved to be highly sensitive in detecting early damage, even when it consists of small stiffness reductions that do not impair the safety or use of the structure, and highly robust to false detections. The analysis and validation allowed concluding that the ability to identify early damage, imperceptible in the original signals, while avoiding observable changes induced by variations in train speed or temperature, was achieved by carefully defining the modelling and fusion sequence of the information. A single-value damage indicator, proposed as a tool for real-time structural assessment of bridges without interfering with the normal service condition, proved capable of characterizing multi-sensor data while being sensitive to identify local changes.

[1] Ph.D. Student, CONSTRUCT-LESE, Faculty of Engineering, University of Porto, Portugal, ameixedo@fe.up.pt
[2] Researcher, LNEC, Laboratório Nacional de Engenharia Civil, Portugal, josantos@lnec.pt
[3] Adjunct Professor, CONSTRUCT-LESE, School of Engineering, Polytechnic of Porto, Portugal, drr@isep.ipp.pt
[4] Full Professor, CONSTRUCT-LESE, Faculty of Engineering, University of Porto, Portugal, ruiabc@fe.up.pt
[5] Full Professor, Department of Structural Engineering, University California San Diego, USA, mdtodd@ucsd.edu

Keywords: damage detection; unsupervised learning; Structural Health Monitoring; traffic-induced dynamic responses; autoregressive models; PCA; regression.

1. Introduction

Bridge maintenance is vital to the structural integrity and cost-effectiveness of any transportation system, and, therefore, the detection of early structural changes or damage plays a central role in any maintenance programme [1]. Although the large majority of bridges is assessed through periodical visual inspections, these are expensive, scattered in time and prone to error, which motivated the wide application of Structural Health Monitoring (SHM), especially in large newly built bridges [2]. Hence, the need to define warning strategies and systems to minimize the disruption of the network [3].

SHM techniques can follow model-updating or data-driven approaches for damage detection [4]. Model updating consists of fitting a numerical model to experimental data to infer damage-related information that cannot be directly measured on site [4]. Despite their reported accuracy, these techniques have an inherent computational complexity, and the need for user judgement makes them less suitable for real-time SHM [5]. On the other hand, data-driven approaches rely on data mining techniques to extract meaningful information from time series acquired on site [6]. The computational simplicity of these approaches renders them more attractive and cost-effective to implement online damage detection in large-scale structures [7].

Damage identification strategies have been widely classified by literature within a five-level hierarchy [8, 9]: i) damage detection, ii) localization, iii) type, iv) severity and v) lifetime prediction. The present paper addresses the first level of the aforementioned hierarchy through data-driven methods based on train-induced dynamic responses. To fulfil this goal, four main operations need to be employed after the acquisition of data [5]: i) feature extraction, ii) feature modelling, iii) data fusion and iv) feature discrimination.

Feature extraction refers to the process of transforming the time series acquired on site into an alternative information, where the correlation with the damage is more readily observed [10]. Modal or modal-based features are the most common in the literature [11 - 14] due to the advantage of being directly associated with the mass and, more importantly, with structural stiffness, which is expected to change in the presence of damage. In addition, modal quantities also have the advantage of being used for structural design and for assessing the vulnerability of structures to actions and hazards [15, 16]. Regardless of these advantages, Operational Modal Analysis (OMA)-based information can also be considered not sensitive to early damage due to the need of

identifying high order modes shapes, which proves very challenging for real structure monitoring [16]. Symbolic data [17], wavelet components [18] and basic signal statistics are also examples of techniques successfully applied as extractors of damage-sensitive features for both static and dynamic monitoring. However, in applications comprising acceleration measurements, autoregressive (AR) models have been widely reported for several reasons [19 - 22]. One of them is their ability to extract features that are sensitive to damage, as the variation in physical parameters (e.g. stiffness) indicating the existence of damage manifests itself by a variation in the coefficients of the fitted AR models. Moreover, AR models depend solely on the response of the structure, and its parameters reflect the inherent structural properties regardless of the excitation sources and their respective variations [23]. In addition, the computational implementation of these models is fairly simple.

Effective damage detection and SHM techniques face the challenge of distinguishing the measured effects caused by environmental and operational variations (EOVs) from those triggered by damage [24]. Hence, SHM methods that are capable of overcoming this issue must necessarily resort to feature modelling. This operation is crucial for false alarm prevention since environmental effects, such as temperature or operational actions, like trains crossing at different speeds, may impose greater variations than those due to damage. Two approaches are generally found in the literature and in the practice of feature modelling [16]: i) input-output, based on regression methods such as Multiple Linear Regression (MLR) [25, 26] or ii) output-only, based on latent variable methods such as Principal Component Analysis (PCA) [12, 16]. The first removes the effects of the EOVs, establishing relationships between measured actions (e.g. temperature, traffic, wind) and measured structural responses. When monitoring systems do not include the measurement of EOVs, latent variable methods can be employed. These methods are able to suppress independent actions using only structural measurements.

Data fusion focuses on reducing the volume of data while preserving its most relevant information. The fusion process may combine features from a single sensor, features from spatially distributed sensors or even heterogeneous data types. In all situations, the objective of a data fusion process is to reach a new type of information with less volume and greater or similar ability to characterize the measured phenomena, when compared to that achieved when using any of the original information sources alone [27]. The Mahalanobis

distance has been thoroughly used in this context due to its capacity to describe the variability in multivariate data sets [11, 28].

Feature discrimination aims at classifying the features into healthy or damaged. It can be divided into supervised or unsupervised learning algorithms [5]. When training data is available from both undamaged and damaged structures, supervised learning algorithms can be used, such as statistical process control [18] or MLP neural networks [21]. Since data obtained from damaged structures is rare or inexistent, unsupervised learning algorithms have been increasingly observed in the literature. Novelty detection methods are the primary class of algorithms used in this situation. This type of algorithm is a two-class problem that indicates if the acquired data comes from normal operating conditions or not [29]. Due to its simplicity and effectiveness, outlier analysis is a broadly implemented novelty detection technique [7, 30], which consists of fitting a probability distribution to the normal condition data and then testing whether the new data complies with the same distribution.

While the majority of SHM works rely on responses derived from ambient vibrations or actions such as temperature and static effects induced by live loads, recent works have also been using the structural responses generated by traffic on bridges to take advantage of the repeatability of these actions, their known behaviour and their great magnitude. Cavadas et al. [25], gathered data on the displacement and rotation along a beam frame subjected to an unknown moving load. Principal component and Robust regression analysis were used to reduce dimensionality. Afterwards, data gathered during a baseline period were used to characterize the natural variation of the parameters, so that subsequent variation beyond this baseline range could be flagged as damage. The method successfully detected stiffness reductions of 20 % in a beam element 30 cm long. However, only a single load was considered, as well as a controlled load speed and a quasi-static behaviour, which are seldom the case in real bridges. Gonzalez & Karoumi [30] proposed a model-free damage detection method that uses deck accelerations and bridge weigh-in-motion data to train a machine learning setup based on ANN and a Gaussian process to classify the data as healthy or damaged. The method was further developed by Neves et al. [31] using a three-dimensional bridge model. One of the limitations found for the proposed strategy was the fact that it did not consider the EOVs on the damage detection process. Nie et al. [32] applied a damage detection approach using two sensors on beam bridges subjected to moving loads and defined a local damage index based on the cross-correlation between the measured responses. To demonstrate the feasibility of the proposed approach, a simply supported beam bridge subjected to a moving mass was simulated and verified using a laboratory prototype. However, it was found that the method always generates several false

positives, revealing the need for further numerical simulations to make it efficient in practical applications. Azim & Gül [22] presented a sensor-clustering-based time series analysis method for continuous global monitoring of girder-type railway bridges using operational data. The method consisted of applying an autoregressive moving average model with exogenous inputs to analyse the free vibration response of the bridge in order to extract damage features. The main limitations pointed out by the authors were the linear nature of the methods used and the influence of changes in environmental conditions, which were not considered in their study.

Despite the widespread research in this field, successful implementations of SHM in bridges based on traffic-induced dynamic responses are still scarce. In most damage detection methodologies that have been proposed, the EOVs in the structural response are often disregarded, the validation of the related methodologies is still performed using numerical simulations on simple structural elements, the type of damages is limited, and the loading scenarios are very specific, which limits their usability in real and complex bridges. In this context, the main contributions of this paper include applying a hybrid combination of machine learning techniques to transient signals, as well as using a digital twin to generate surrogate responses in multiple scenarios. Up to this date, the transient signals have not been used efficiently and robustly for damage detection. These signals, resulting from train crossings, correspond to an important mass travelling at significant speeds, thus generating features that can hide those associated with damage. The set of techniques used herein allows removing all the train-related features to expose, with high sensitivity, those generated by damage. This approach takes advantage of the large magnitude of the signals and the small influence of temperature and time dependent structural effects, which produce bias and reduce the sensitivity of the majority of the damage identification techniques that rely on long-term trends.

The following original milestones are achieved with this research work:

- the development of an original data-driven unsupervised damage detection methodology, capable of automatically extracting compact and meaningful information related to the condition of the bridge using acceleration responses induced by traffic;
- the improvement of the sensitivity of the features using large magnitude signals resulting from the passage of trains, which impose a greater excitation of the bridge in a short-time, when compared with ambient or static loads;

- the decrease in the influence of slow environmental actions, such as temperature and humidity, as well as material properties, such as shrinkage, creep and relaxation, by acquiring signal in short periods of time, as opposed to continuous monitoring;
- the development of a methodology capable of detecting damage based on responses that can be measured without interfering with the normal service condition of the structure;
- prove the importance of feature modelling by showing the supremacy of the EOVs when compared to damage;
- show the importance of multi-sensor data fusion to enhance the detection of early-damages;
- the validation of the methodology using a highly reliable digital-twin of a complex railway bridge.

2. Damage detection methodology

2.1 Overview

The unsupervised data-driven SHM methodology proposed in this paper for detecting damage in bridges, based on traffic-induced dynamic responses, aims at being robust and generic enough to be applied to any type of bridge, and entails the four operations shown in Figure 1: i) damage-sensitive feature extraction from the acquired structural responses, ii) feature modelling to remove EOVs, iii) data fusion to merge multi-sensor features without losing damage-related information, and, iv) feature discrimination to classify the extracted features in two categories, healthy or damaged.

Feature extraction is addressed in this paper using AR models. The AR models are fitted to the acceleration responses of the monitored structure, and their parameters are extracted resulting in as many sets of multivariate data as the number of sensors installed. Afterwards, the suppression of thermal and operational variations is conducted following the two alternative approaches, one based on both actions and structural response measurements and the other based on structural response measurements alone. This is accomplished through the parallel implementation of two well-known multivariate statistical tools: the MLR for the first approach, and the PCA for the second approach. In order to improve sensitivity, a Mahalanobis distance is applied to the modelled features, allowing for an effective fusion, first of the features from each sensor and, in a second stage, of the multi-sensor information. The outcome is a damage indicator, DI, for each train crossing. In the last stage, an outlier analysis is implemented to automatically discriminate each DI into healthy or damaged, using a statistical confidence boundary, CB, based on the Gaussian inverse cumulative distribution function.

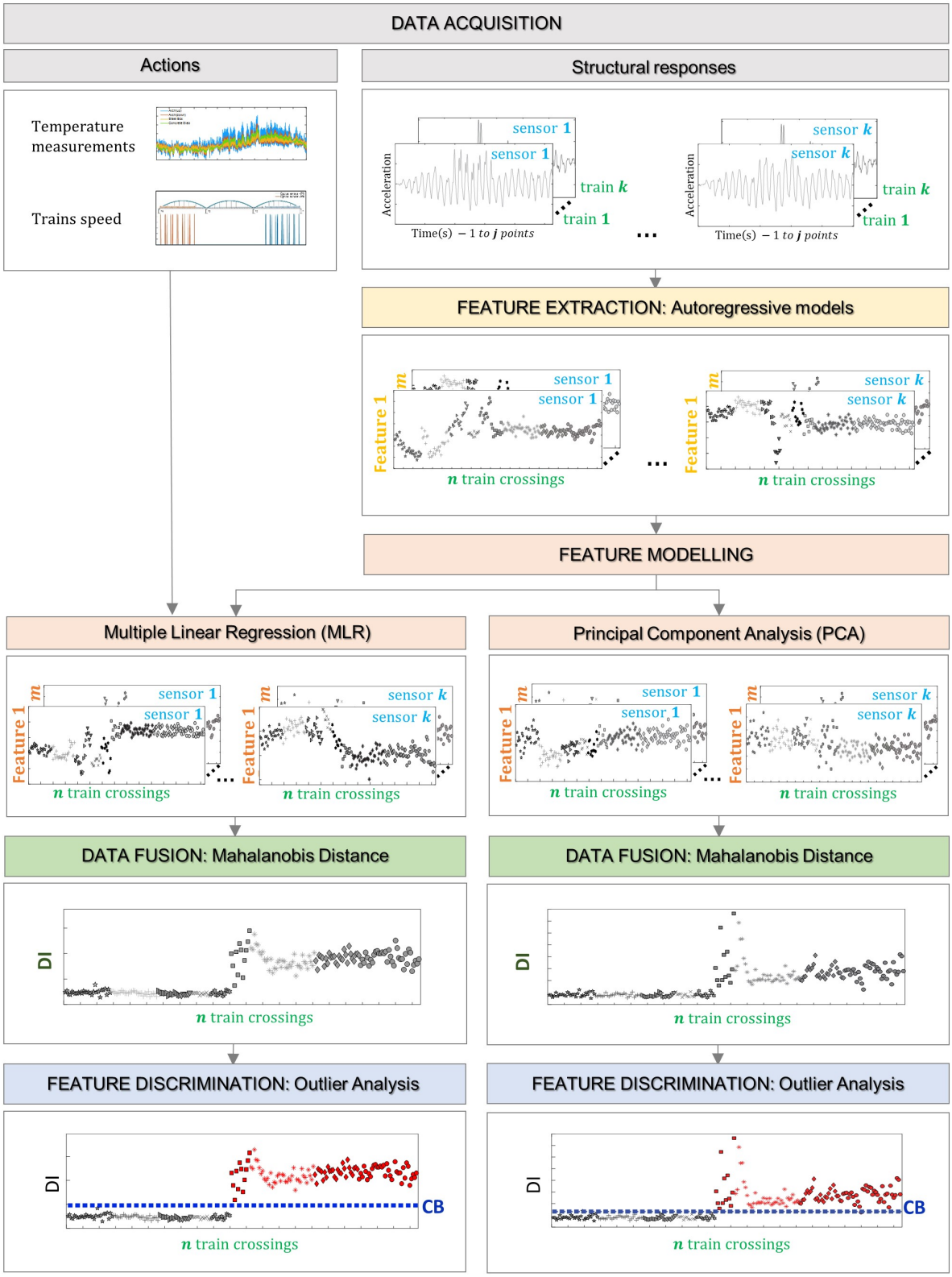

Figure 1. Flowchart of the damage detection methodology

Although this methodology comprises a set of baseline features to define the CB, it is considered unsupervised, since the responses acquired to build this baseline regard the state condition of the bridge at the time it begins to be monitored, which does not necessarily correspond to an undamaged state. For either existing or new bridges, regardless of their geometry, the only data needed to implement this methodology is the train

crossing signals for one or more types of trains at their different operating speeds and for several temperatures. As a consequence, structural changes signalled by the methodology comprise progressive damages in relation to the condition defined during the baseline. In addition, and more importantly, one of the great advantages of the methodology is the speed at which the baseline can be defined. It can be promptly established during one day for several types of trains with different loads crossing the bridge. The environmental effects can also be considered, since the weather (temperature and wind) varies according to the time of day.

A theoretical background of each technique implemented in the methodology is summarized in the following subsections.

2.2 Feature extraction

Within the SHM realm, time series analysis is a statistical tool that attempts to fit a mathematical model to time series data to extract meaningful information. Among the different types of time series models, the AR model is known as the most widely used to extract damage-sensitive features [33].

The $AR(m)$ model, where m defines the order or number of parameters in the model, is developed from response time-series data $x_1, x_2, \dots, x_n$ and can be written as:

$$x_j = \sum_{i=1}^{m} a_i x_{j-i} + \varepsilon_j \tag{1}$$

Here the current value of the response, x_j, is defined as a linear combination of the m previous response values multiplied by AR constant parameters a_i. Quantity ε_j is an unobservable random error (or residual error) in signal value j. This quantity implies the difference between the measured time series and the predicted one obtained by the AR model [5].

The idea is that in a system where different dynamic frequency contents are present at different times, the estimated parameters a_i should change between intervals [34]. The process of extracting the AR parameters is based on fitting the AR model to each vibration time-domain response acquired from each sensor in undamaged and damaged conditions. The vectors of the model parameters in the baseline and in the damaged state condition are then used as damage features.

In a matrix format, the AR model can be represented by:

$$\begin{bmatrix} x_{m+1} \\ x_{m+2} \\ \vdots \\ x_n \end{bmatrix} = \begin{bmatrix} x_1 & x_2 & \cdots & x_m \\ x_2 & x_3 & \dots & x_{m+1} \\ \vdots & \vdots & \ddots & \vdots \\ x_{n-m} & x_{n-m+1} & \cdots & x_{n-1} \end{bmatrix} \begin{bmatrix} a_m \\ a_{m-1} \\ \vdots \\ a_1 \end{bmatrix} + \begin{bmatrix} \varepsilon_{m+1} \\ \varepsilon_{m+2} \\ \vdots \\ \varepsilon_n \end{bmatrix} \tag{2}$$

Typical time series lead to an overdetermined set of equations that must be solved to obtain estimates of the AR coefficients. There are several methods that can be used to solve the coefficients, including the Yule-Walker approach or the least-squares method [35].

2.3 Feature modelling

2.3.1 Multiple Linear Regression

The MLR model is the most straightforward multivariate statistical tool used in the realm of feature modelling SHM data. Despite the fact that it assumes linear relations between environmental / operational actions and structural response measurements, its theoretical and computational simplicity, combined with the fact that most physical relations are linear in nature, make it appealing for normalization. However, it is necessary to measure the environmental and operational actions in order to remove them from the structural responses or features.

In this paper, the MLR model uses a set of measured train speeds and bridge temperatures as inputs and delivers a matrix output that represents the estimated (or predicted) AR parameters. Given m AR parameters, n baseline simulations and s operational / environmental actions, the multivariate regression model is expressed by the following [36]:

$$Y = X \cdot \hat{w} + \varepsilon_{MLR} \tag{3}$$

where X is the *n-by-(s+1)* input temperature and speed matrix, $\hat{w}$ is a *(s+1)-by-m* matrix of coefficients that weights each environmental / operational input, ε_{MLR} is the *n-by-m* regression error and Y is an *n-by-m* output matrix of predicted AR parameters. The coefficients of the model parameters $\hat{w}$ are obtained through the least squares method and given by the following equation:

$$\hat{w} = (X^T \cdot X)^{-1} \cdot X^T \cdot Y \tag{4}$$

Once the model is calibrated, i.e. the optimal weights are evaluated, new data can be used as input ($\hat{X}$) and the residual error matrix $\hat{\varepsilon}_{MLR}$, which corresponds to the damage-sensitive features from which the environmental and operational effects are removed, is denoted by:

$$\hat{\varepsilon}_{MLR} = Y - \hat{X} \cdot \hat{w} \tag{5}$$

This procedure is repeated for the parameters of each sensor.

2.3.2 Principal Component Analysis

One of the main obstacles in the application of vibration-based SHM systems under operational conditions is the difficulty to remove the EOVs from the dynamic responses without measuring them, in order to obtain features that are mainly sensitive to damage. To overcome this problem, PCA is used [11]. PCA is a multivariate statistical method that allows obtaining, from a group of correlated variables, a set of linearly uncorrelated vectors called principal components or scores. Assuming that environmental conditions have a linear effect on the identified parameters, the PCA of continuous monitoring results can efficiently remove the effects of the EOVs [11, 37, 38].

Considering an *n-by-m* matrix X with the original features extracted from the dynamic responses, where m is the number of AR parameters and n is the number of simulations for the baseline condition, a transformation to another set of m parameters, Y, designated as principal components or scores, can be achieved by the following equation:

$$Y = X \cdot T \tag{6}$$

where T is an *m-by-m* orthonormal linear transformation matrix that applies a rotation to the original coordinate system. The covariance matrix of the AR parameters in the baseline condition, C, is related to the covariance matrix of the scores, Λ, as follows:

$$C = T \cdot \Lambda \cdot T^T \tag{7}$$

where T and Λ are matrixes obtained by the singular value decomposition of the covariance matrix C of the AR parameters. The columns of T are the eigenvectors and the diagonal matrix Λ comprises the eigenvalues of the matrix C in descending order. Hence, the eigenvalues stored in Λ are the variances of the components of Y and express the relative importance of each principal component in the entire data set variation [11].

As demonstrated by Santos et al. [16], the PCA is able to retain meaningful information related to environmental and operational effects in the first axes, whereas variations related to other small magnitude effects, such as damage, may be summarized in latter axes. Since the aim of the present work is to detect damage, which generally has a local character, the feature modelling procedure consists, thus, in removing the most significant principal components from the features and retaining the remaining ones for subsequent statistical analysis. With this in mind, the matrix Λ can be divided into a matrix with the first p eigenvalues and a matrix with the remaining *m-p* eigenvectors. Defining the number of p components remains a challenge when

it comes to the truthful interpretation of multivariate data. Although several approaches have been proposed, there is still no definitive answer [39]. In this work, the value of p (or the number of PCs to discard) is determined based on the rule of thumb in which the cumulative percentage of the variance reaches 80% [39, 40].

After choosing p, the *m-p* components of the matrix Y can be calculated using Equation (6) and a transformation matrix $\hat{T}$ built with the remaining *m-p* columns of T. Those *m-p* components can be remapped to the original space using the following:

$$F_{PCA} = X \cdot \hat{T} \cdot \hat{T}^T \tag{8}$$

where F_{PCA} is the *n-by-m* matrix of PCA-based features, which are expected to be less sensitive to environmental and operation effects and more sensitive to damage. This procedure is repeated for each sensor.

2.4 Data fusion

The Mahalanobis distance can be applied on estimation errors obtained from MLR or PCA in order to describe the variability present in the normalized features, and can merge features from multiple sensors performing data fusion.

The Mahalanobis distance measures the distance between the baseline features and the damage-sensitive features in order to express the similarities between them, with shorter distances representing greater similarities. The Mahalanobis distance is generic enough to be used to detect any damage scenario, while providing a weighting that is entirely unsupervised, and therefore independent of human intervention, the type of structure, and the actions imposed on it. It consists of a weighted damage indicator in which the weights are determined by the covariance structure. In addition, and more importantly, the weighting proportional to the covariance structure provides an additional layer of feature modelling which, when defined for regular actions, allows outlining with high sensitivity those that were not used for the definition of the covariance structure. The analytical expression of the Mahalanobis distance for each simulation i, denoted as DI_i, is the following:

$$DI_i = \sqrt{(x_i - \bar{x}) \cdot {S_x}^{-1} \cdot (x_i - \bar{x})^T} \tag{9}$$

where x_i is a vector of m features representing the potential damage/outlier, $\bar{x}$ is the matrix of the means of the features estimated in the baseline simulations, and S_x is the covariance matrix of the baseline simulations.

The Mahalanobis distance is computed for each simulation and each sensor resulting in a matrix with n Mahalanobis distances for k sensors, where n is the total number of simulations. Afterwards, a new Mahalanobis distance can be applied in order to obtain a vector *n-by-1* merging the information from all the sensors and providing a DI for each simulation. When data from a structural state that differs from the baseline is tested, the DI value is expected to increase substantially.

2.5 Feature discrimination – Outlier Analysis

Generally, the literature assumes that the Mahalanobis squared distance can be approximated by a chi-squared distribution in *n*-dimensional space, thus the Mahalanobis distance can be approximated by a normal (or Gaussian) distribution and an outlier analysis can be performed based on a statistical threshold [20, 41, 42]. Under this hypothesis, a confidence boundary (CB) to detect a DI that constitutes an outlier can be estimated by the Gaussian inverse cumulative distribution function (ICDF) considering a mean μ and standard deviation σ of the baseline feature vector, and for a level of significance α. The inverse function can be defined in terms of the Gaussian cumulative distribution function (CDF) as follows:

$$CB = invF(1-\alpha) \tag{10}$$

where

$$F(x|\mu,\sigma) = \frac{1}{\sigma\sqrt{2\pi}}\int_{-\infty}^{x} e^{-\frac{1}{2}\left(\frac{x-\mu}{\sigma}\right)^2}\, dy, for\ x\epsilon\mathbb{R} \tag{11}$$

Thus, a feature is considered to be an outlier when its DI is equal or greater than CB. It is important to note that the selection of α carries a trade-off between the Type I error (*false-positive* indication of damage) and the Type II error (*false-negative* indication of damage) [5].

3. Case study: The Sado Railway Bridge

3.1 Structural System

The case study used to test and validate the strategy and techniques proposed herein is the bowstring arch bridge over the Sado River, located on the southern line of the Portuguese railway network that establishes the connection between Lisbon and the Algarve (Figure 2). The structure is prepared for conventional and tilting passenger trains with speeds up to 250 km/h, as well as for freight trains with a maximum axle load of 25 t.

Figure 2. Overview of the Sado Bridge [43].

The bridge has a total length of 480 m, divided into 3 continuous spans, each with 160 m, and is part of a longer structure that includes the North access viaduct, with 1115 m, and the South access viaduct with 1140 m. As shown in Figure 3, the bridge is suspended from three arches connected to each span of the deck by 18 hangers distributed over a single plane on the axis of the structure. The superstructure has a steel-concrete composite deck, while the substructure, which includes four piers, the abutments and the pile foundations, is made of reinforced concrete. At the top of each pier, there are two spherical and multidirectional steel sliding bearing devices, 4 m apart. The bearing devices have a circular contact surface, with a 910 mm diameter at piers P1 and P4, and a 1300 mm diameter at piers P2 and P3, and include an antifriction layer in XLIDE material. The deck is fixed on pier P1, whereas on piers P2, P3 and P4 only the transverse movements of the deck are restrained, while the longitudinal movements are constrained by seismic dampers. Figure 3 also shows a scheme of the location and typology of each bearing device.

Figure 4 details the deck, the arches, pier P2 (identical to pier P3) and its foundations through a cross-section and a front view. The bridge deck consists of a concrete slab laid over a U-shaped steel box girder. The three parabolic arches have a hexagonal hollow cross-section, with a variable width increasing towards the top. The connection between the deck and the hanger is performed through spherical hinges that allow the torsional rotation of the deck. The suspension of the deck loads is performed by the hangers by means of steel diaphragms and two diagonal strings at each connection. On the other side, the hanger-to-arch connection is performed by means of an eye-plate also with a spherical hinge and a special cast steel piece. At each point of intersection, the arch is featured with transverse diaphragms, which increase the overall stiffness and limit the distortion of the section. Regarding the piers, each one has a hexagonal hollow cross-section and rests on heads of reinforced concrete piles with lengths up to 50 m and 2 m diameters. Pier heads P1 and P4 are formed by nine piles, while pier heads P2 and P3 are formed by twelve piles.

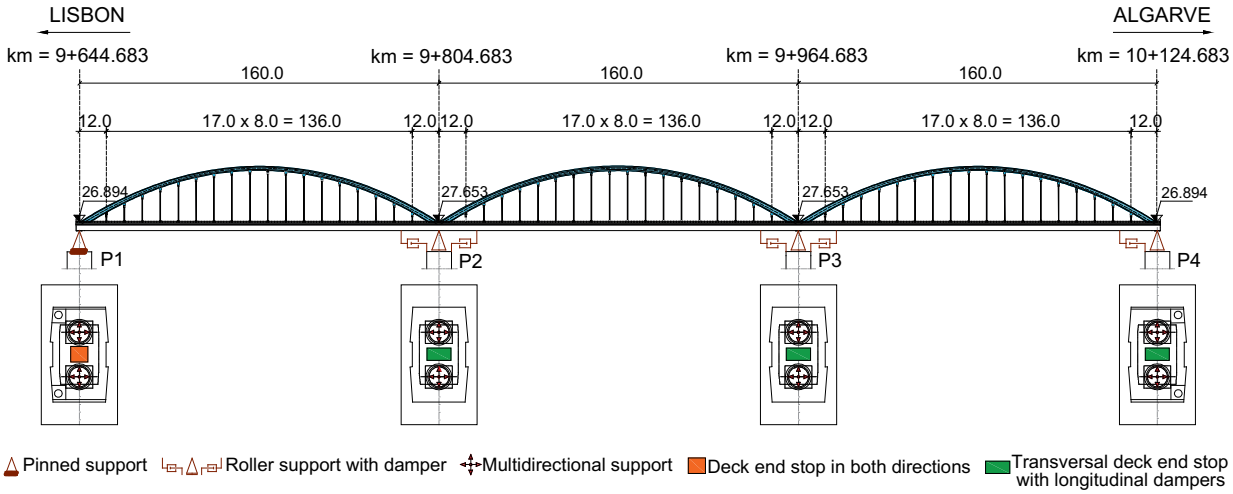

Figure 3. Lateral view of the bridge with a detail from the bearing devices (adapted from GRID et al. [44]).

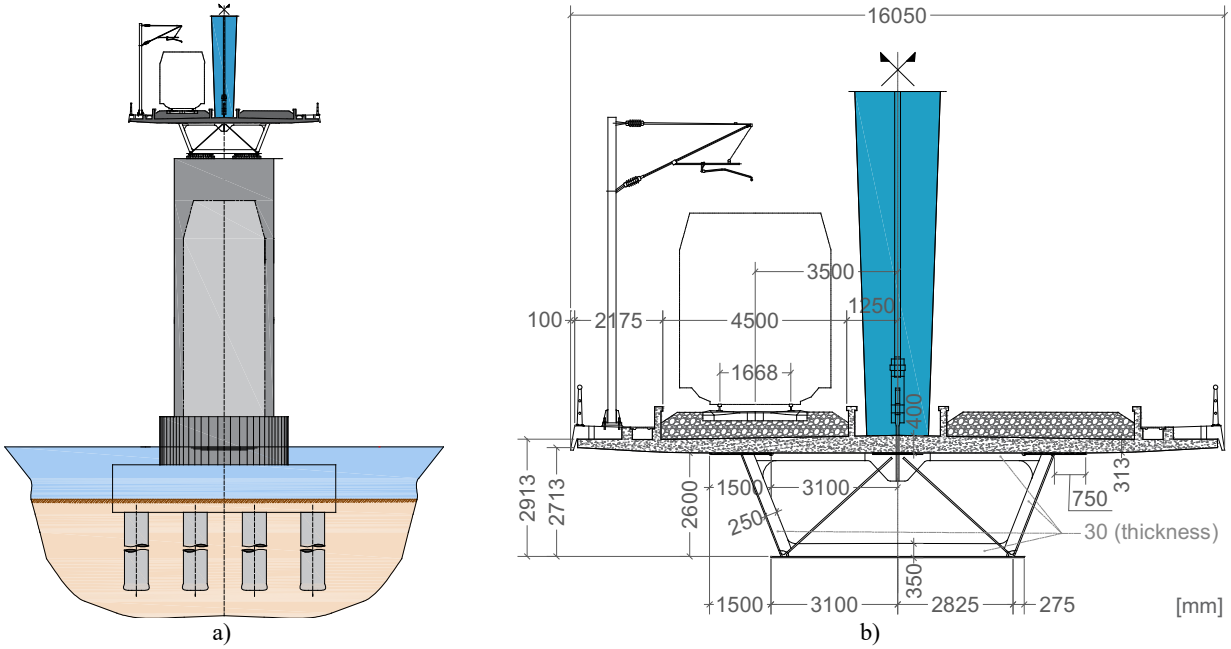

Figure 4. Sado Bridge details: a) front view, b) cross-section of the deck (adapted from GRID et al. [44]).

3.2 Monitoring System

The structural health condition of the Railway bridge over the Sado River has been controlled with a comprehensive autonomous online monitoring system (Figure 5a) since the beginning of its life cycle.

To identify each train that crosses the bridge and compute its speed, two pairs of optical sensors were installed at both ends of the bridge (Figure 5b). The structural temperature action is measured using NTC thermistors and PT100 sensors. Twelve NTC thermistors were installed in three sections of the arch. Additionally, the measurements from four NTC thermistors fixed to the steel box girder and three PT100 sensors embedded in the concrete slab were also acquired (Figure 5d).

To control the behaviour of the bearing devices, the responses from longitudinal displacement transducers were obtained from eight sensors, each adjacent to a bearing device (Figure 5b).

The set of sensors also includes one vertical piezoelectric accelerometer fixed at the mid-span of the concrete slab, two triaxial force balance accelerometers at the thirds of the mid-span steel box girder, and twelve vertical force balance accelerometers fixed along each span of the steel box girder (Figure 5c). Four longitudinal MEMS DC accelerometers were also installed at the top of each pier (Figure 5b). Data acquisition is carried out continuously by a locally deployed industrial computer in order to save the time history while the train is crossing, at a sampling rate of 2000 Hz.

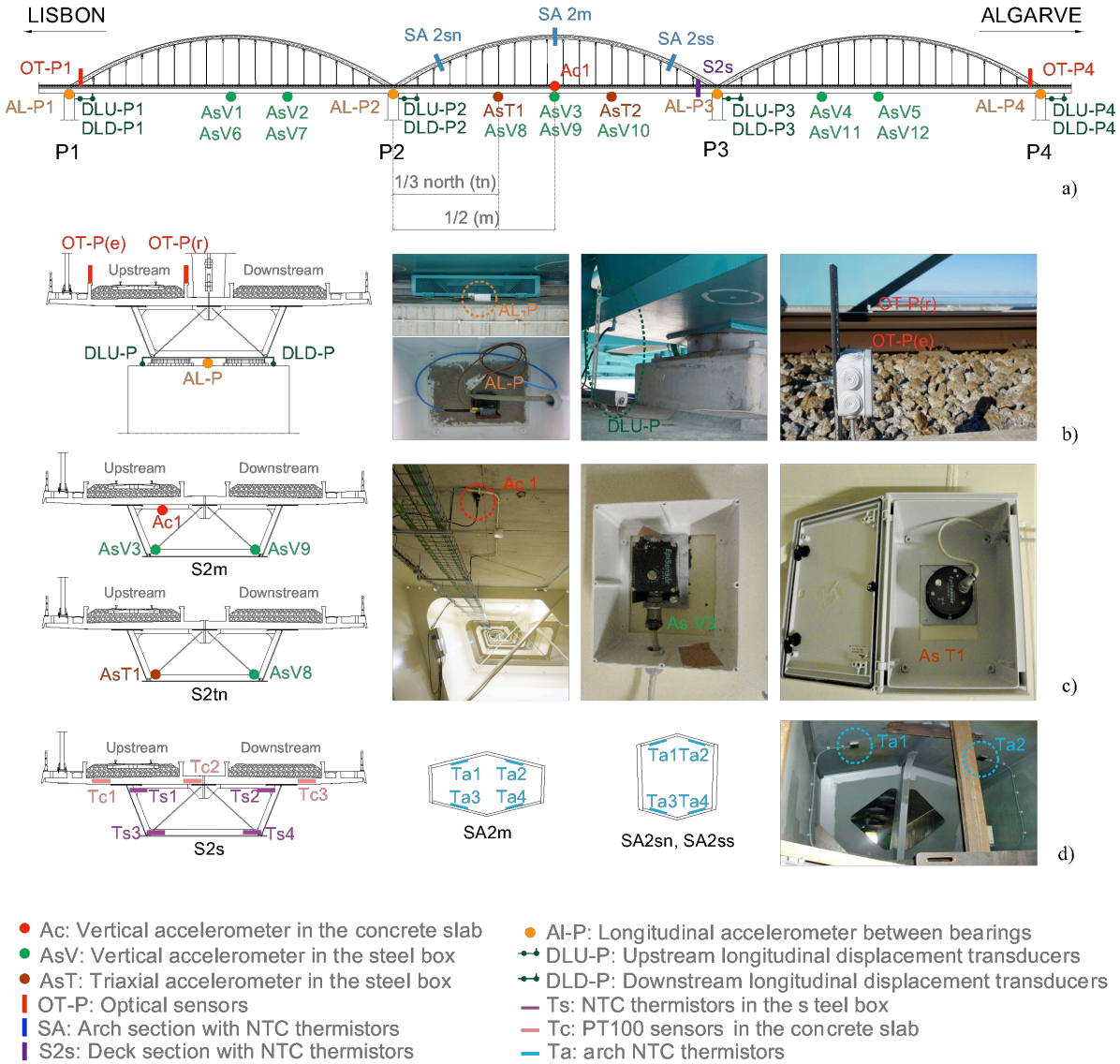

Figure 5. SHM system installed in the Sado railway bridge: a) overview, b) displacement transducer, optical sensor and longitudinal accelerometer, c) vertical accelerometers and d) NTC thermistors and PT100 sensors.

4. Realistic simulation of damage scenarios

4.1 FE Numerical model

A realistic simulation of healthy and damage scenarios was conducted in order to test and validate the strategies proposed herein, since it was not possible to simulate damage scenarios experimentally. After a successfully validation of the methodology, it can be applied directly to experimental data from different types of bridges, where a baseline scenario is defined and further experimental data can be tested to detect the occurrence of eventual structural changes.

For this purpose, a 3D finite element (FE) numerical model of the bridge was developed in ANSYS software [45]. The deck, hangers and arches were previously modelled by Albuquerque et al. [46] and an upgrade of the numerical model was developed in the present research work to include the track, the bearings, the piers and the foundations. Figure 6 illustrates the numerical model and a schematic representation highlighting the different types of finite elements applied.

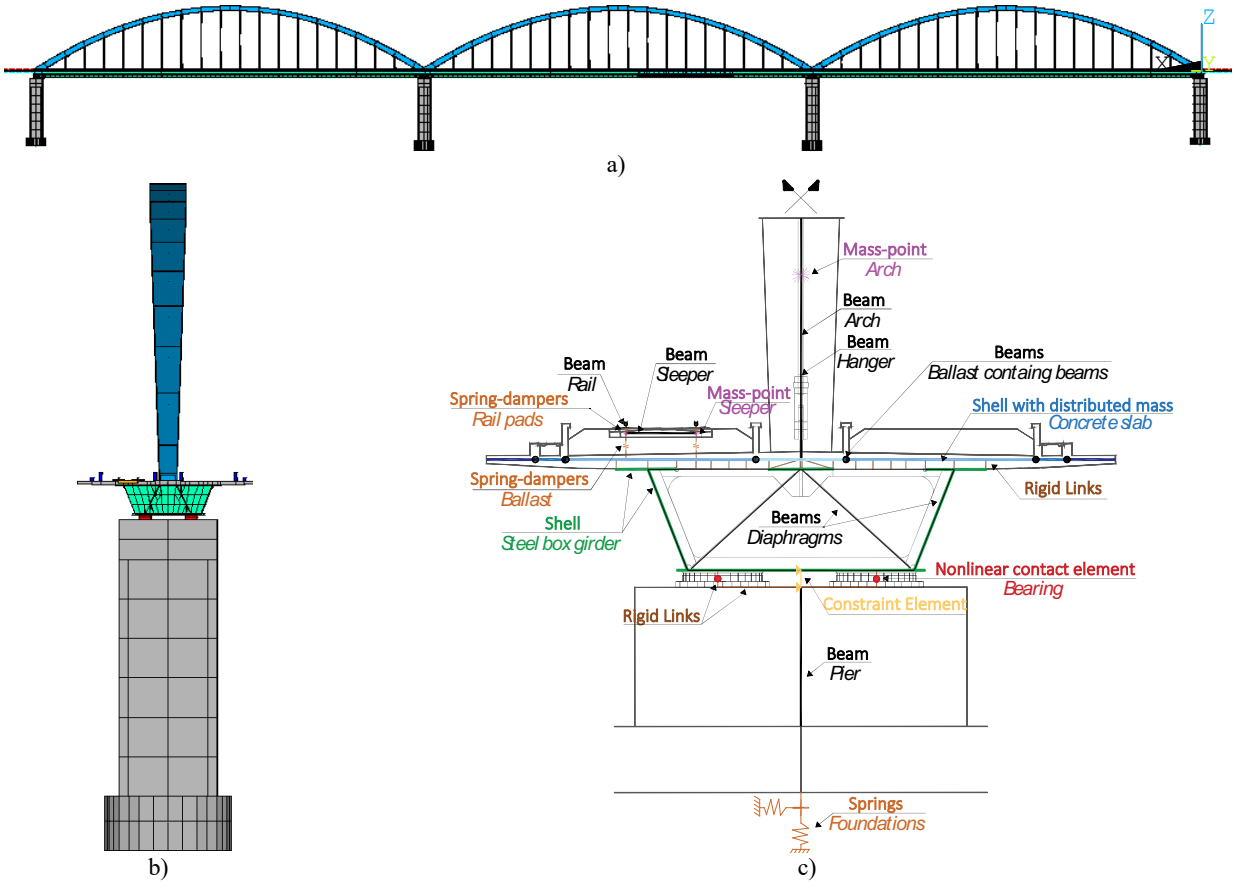

Figure 6. 3D Numerical model of the Sado railway bridge: a) lateral view, b) frontal view, c) cross-section schematic with the finite elements applied.

Among the modelled structural elements, those defined as beam finite elements consist of piers, sleepers, ballast-retaining walls, rails, arches, hangers, transverse stiffeners, diaphragms and diagonals. Shell elements

were used to model the concrete slab and the steel box girder, while the pads, the ballast layer and the foundations were modelled using linear spring-dashpot assemblies. The mass of the non-structural elements and ballast layer was distributed along the concrete slab. Concentrated mass elements were used to reproduce the mass of the arches' diaphragms and the mass of the sleepers simply positioned at their extremities. The connection between the concrete slab and the upper flanges of the steel box girder, as well as the connection between the deck and the track, were performed using rigid links.

A special emphasis was given to the bearing devices, since they can strongly influence the performance of the bridge. Hence, in order to simulate the sliding behaviour of the bearings, nonlinear contact elements were applied. Additionally, constraint elements located between the bearings were used to restrict the transversal movement in each pier, and both longitudinal and transversal movements in the case of the first pier. It should be noted that the seismic dampers were not modelled, since they are not activated during serviceability loads, such as the ones caused by train passages or environmental actions. The numerical model of the bridge includes 25924 nodes and 38620 finite elements.

The deck's steel was defined with a modulus of elasticity of 210 GPa, a Poisson's ratio of 0.3 and a density of 7850 kg/m^3, while the concrete slab and piers have a density of 2500 kg/m^3, a Poisson's ratio of 0.15 and a modulus of elasticity of 43 GPa based on the updated model presented by Albuquerque et al. [46]. The arches were composed of variable cross-sections, with varying thickness, width and height, both of flanges and webs. The piers were defined considering three different types of reinforced concrete cross-sections, namely a solid rectangular section, a rectangular hollow-section and an elliptical hollow-section.

The bearing devices were modelled using nonlinear contact elements CONTA178 [45], which allow contact and sliding between any pair of nodes, and are capable of withstanding compression forces normal to their plane and friction forces along the tangential directions based on the Coulomb model. Their coefficient of friction μ was defined as 1.5% during the numerical analysis, based on the design specifications [43].

The boundary conditions were simulated using the results obtained from in-situ geotechnical tests conducted during the construction of the bridge [43]. An equivalent soil stiffness in each direction was computed and included in the numerical model of the bridge using spring elements. During these calculations, the SPT N-values and the shear wave velocity of the soil (Vs), obtained from the in-situ tests, were considered, along with

the classification of the soil resulting from the laboratory analyses of the samples collected during the same tests.

4.2 Model validation

The dynamic numerical simulations conducted in the present work aimed at reproducing the structural quantities measured in the exact locations of the real sensors installed on site, when a train crosses the bridge. To accurately reproduce these structural responses, the temperature action measured precisely during the passage of each train was introduced as input in the numerical model. Using the measurements of the optical sensors' setup, installed at both ends of the bridge, the train speed and axle configuration were obtained and the type of train was identified. The dynamic analyses mentioned hereinafter were carried out for two of the passenger trains that normally cross the Sado bridge, namely, the Alfa Pendular (AP) train and the Intercity (IC) train. Their common speeds on the bridge are 220 km/h for the AP train and 190 km/h for the IC train. The average axle loads of these trains are presented in Figure 7. Rayleigh damping was considered for the train crossings with the damping matrix computed using the frequencies and damping coefficients identified in an ambient vibration test [47]. The nonlinear problem was solved based on the Full Newton-Raphson method and the dynamic analyses were performed by the Newmark direct integration method, using a methodology of moving loads [48]. The resolution of the dynamic problem involves calculating the dynamic equilibrium equations of the bridge, which includes the time-invariant mass, damping and stiffness matrices of the bridge, and the time-variant vector of the moving forces of the train. The force variation due to the inertial, damping and elastic forces of the vehicle is not considered. The integration time step (Δt) used in the analyses was 0.005 s. The analyses ended two seconds after the vehicle crossed the bridge in order to consider the free vibration period of the structure.

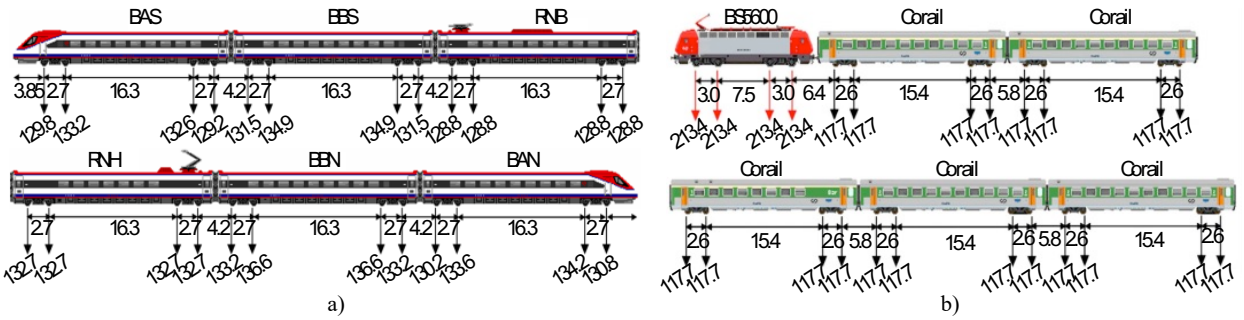

Figure 7. Trains and corresponding loading schemes: a) Alfa Pendular; b) Intercity.

To ensure that the numerical model accurately simulates the structural behaviour of the bridge, the responses obtained from dynamic, modal and static analyses were compared with those measured by the SHM system

[49]. Regarding the dynamic behaviour, numerical simulations were conducted considering the AP train as a set of moving loads crossing the Sado bridge at a speed of 216 km/h. Figure 8 shows a very good agreement between the experimental and numerical responses, in terms of the longitudinal accelerations measured on pier P2 and the vertical accelerations acquired on the concrete slab and on the steel box girder at the second mid-span. Concerning the auto-spectra resulting from the acceleration measurements, the main frequency is repeatedly 2.3 Hz, which corresponds to the passage of equally spaced axle groups of the AP train, illustrating a clear influence of the action on the response of the bridge. Before the comparison, all time-series were filtered based on a low-pass digital filter with a cut-off frequency equal to 15 Hz.

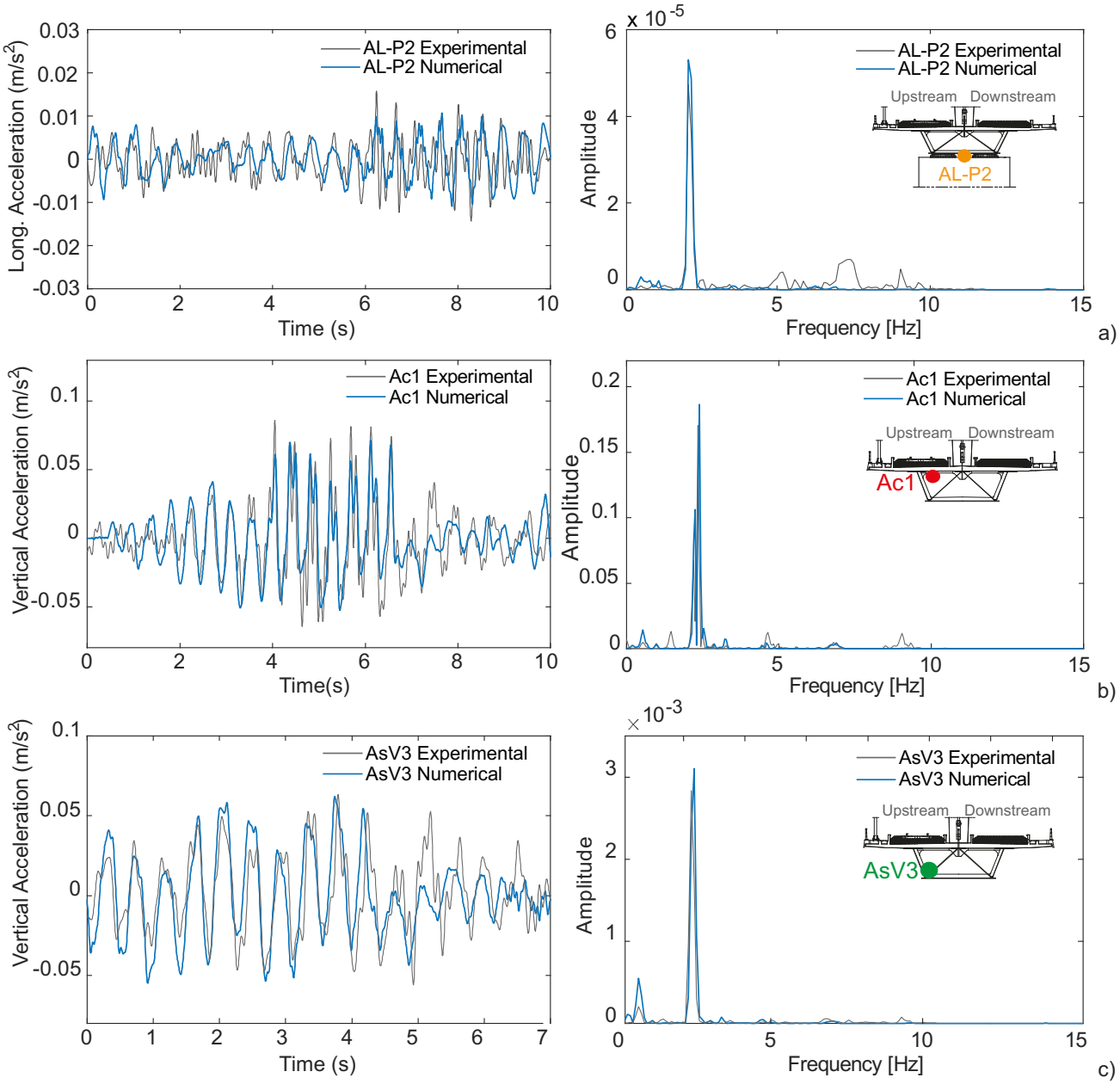

Figure 8. Numerical and experimental accelerations and corresponding auto-spectra, with the Alfa Pendular train at 216 km/h measured by sensors: a) AL-P2, b) Ac1, c) AsV3.

The numerical natural frequencies were also compared with those obtained experimentally during an ambient vibration test [47]. Figure 9a shows a very high coefficient of determination (R^2=0.9993) between the numerical and the experimental results. To validate the static behaviour of the numerical model, the response of the structure to the action of temperature was studied. Figure 9b presents a very good agreement between the numerical and experimental displacements of pier P4 for the temperature measured on site between November 2015 and November 2016.

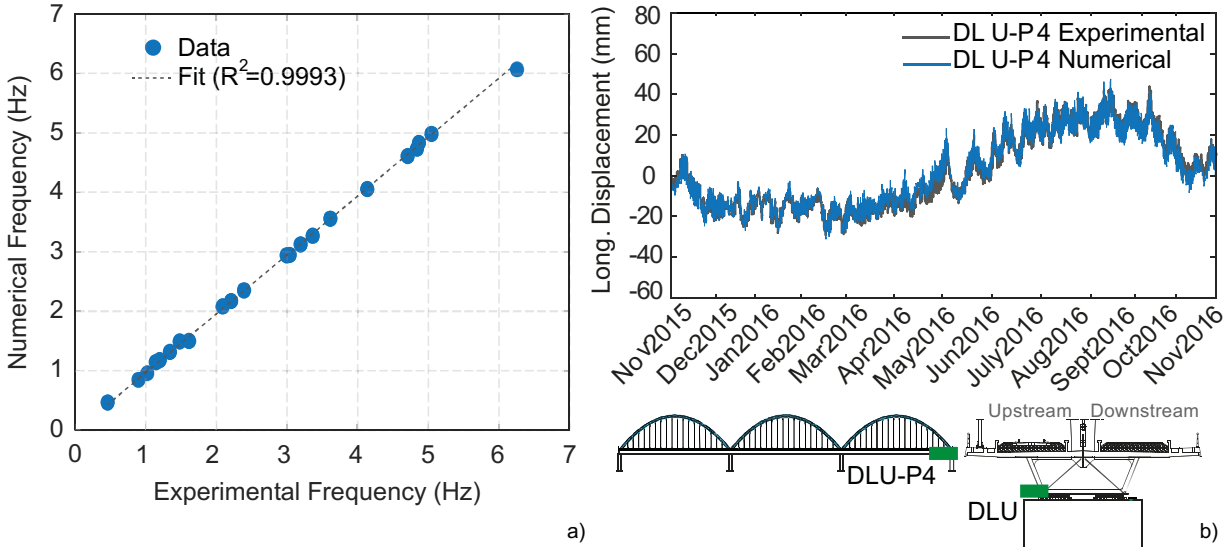

Figure 9. Numerical model validation: a) agreement between numerical and experimental modal frequencies, b) static validation of the displacements measured on pier P4.

4.3 Damage scenarios

To test the methodology proposed in Section 2, the structural response of the Sado bridge during the passage of the AP and IC trains, was replicated for the 23 accelerometers shown in Figure 5 using time-history numerical simulations comprising several realistic scenarios, for both baseline and damaged conditions.

Figure 10 summarizes the 100 simulations of the baseline (undamaged) condition that aim at reproducing the responses of the bridge taking into account the variability of temperature, speed, loads and type of train. These baseline scenarios compose the training dictionary and do not include any damage on any location.

During each simulation, real temperatures measured by the SHM system were introduced in the elements of the bridge. The average values for each season were 21ºC for spring, 30ºC for summer, 16ºC for autumn and 10ºC for winter, but the dispersion across the structure was considered by measuring and using temperature values in all elements of the bridge. The simulations included the AP and IC trains (Figure 7) crossing the bridge with ten different loading schemes, according to the experimental observations previously made by Pimentel et al. [50]. Three train speeds were considered for each type of train, as observed in Figure 10, thus

resulting in 100 time-history simulations for the baseline condition, each taking approximately 10 hours on a 4.2 GHz Quad-Core desktop with 32.0 GB of RAM.

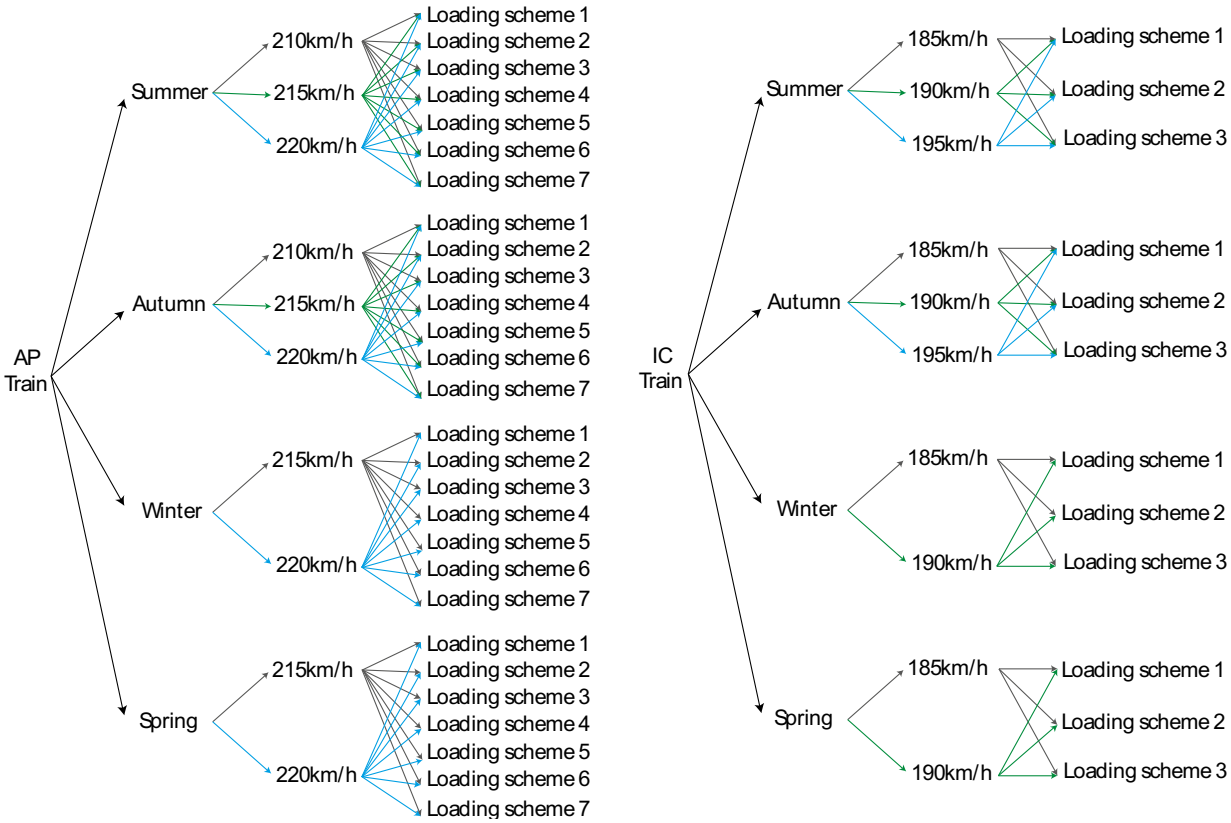

Figure 10. Combination of 100 simulations for the baseline condition.

The damage scenarios were chosen based on possible vulnerabilities identified for the type of structural system, taken into account its materials, connections, behaviour and loadings [51]. Among the several scenarios that can be considered, those related to friction increments in mechanical moving elements of the structural system, such as the bearing devices, as well as those associated with corrosion in structural and reinforcing steel and cracking of concrete were assumed as the most likely [51–54] and, therefore, simulated to validate the techniques presented herein. While friction increments were simulated in all bearing devices, cracking and corrosion were considered in several sections across the structure, so as to ensure a good representativeness. Hence, damage scenarios were simulated, along with dynamic traffic loading, according to four different groups: i) damages in the bearing devices (D1), ii) damages in the concrete slab (D2), iii) damages in the diaphragms (D3) and iv) damages in the arches (D4).

The locations of each type of damage are illustrated in Figure 11. Each scenario was simulated considering only one damage location. Nevertheless, if, by any chance, two or more damage scenarios in different locations are observed at the same time, the effects from multiple damage locations are expected to superimpose, and the

influence on the features extracted from the data will be greater. Therefore, the multiple damage scenario will be more observable than the scenarios tested here. Regarding the damage of type D1, it was simulated as a discrete damage and four severities were included, namely, the increase of the friction coefficient from a reference value of 1.5% to 1.8%, 2.4%, 3.0% as well as the full restrain of movements between the pier and the deck. The remaining damage scenarios consisted of 5%, 10% and 20% stiffness reductions in the chosen sections of the bridge (Figure 11). The damage type D2 consisted of a stiffness reduction in the cross section of the concrete slab comprising a 2 m length of the bridge and a damage-to-span length ratio of 1.25%. The damage type D3 involved a local stiffness reduction comprising one diaphragm. For each location of the damage type D4, a stiffness reduction was applied in an arch extension of 8 m, which represents 4.7% of the arc length. These structural changes were simulated by reducing the modulus of elasticity of the concrete (type D2) and the steel (types D3 and D4). Thus, a total of 114 damage scenarios were simulated for AP train crossings at 220 km/h, using the loading scheme presented in Figure 7a and adding as input the temperatures measured on site during a summer day. Additional damage scenarios could have been simulated for different combinations of EOVs. However, as observed in section 5.3, the proposed methodology is effective in removing these effects and keeping only those generated by structural changes.

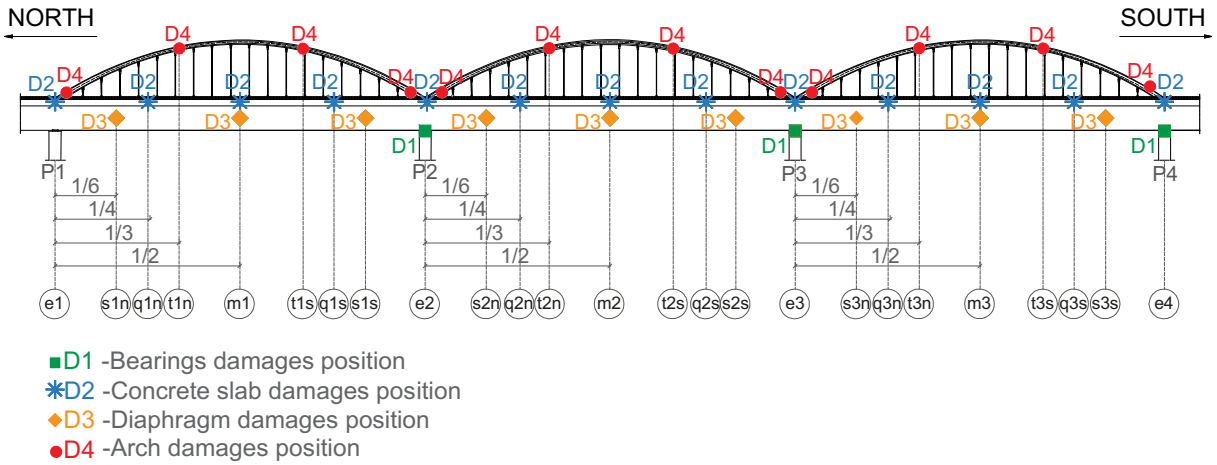

Figure 11. Types of damages and their location on the Sado bridge.

To obtain the most similar and reliable reproduction of the real SHM data, the noise measured on site by each accelerometer was added to the corresponding numerical output. These noise distributions were acquired while no trains were travelling over the bridge and on non-windy conditions. Each simulation was polluted with different noise signals acquired on different days, thus ensuring the most accurate validation of the techniques developed herein. Figure 12 presents an example of a vertical acceleration response of the bridge at the second

mid-span of the concrete slab for an AP train crossing, before and after being corrupted. The noise distribution applied to the response, which was measured by sensor Ac1 of the SHM system, is also shown.

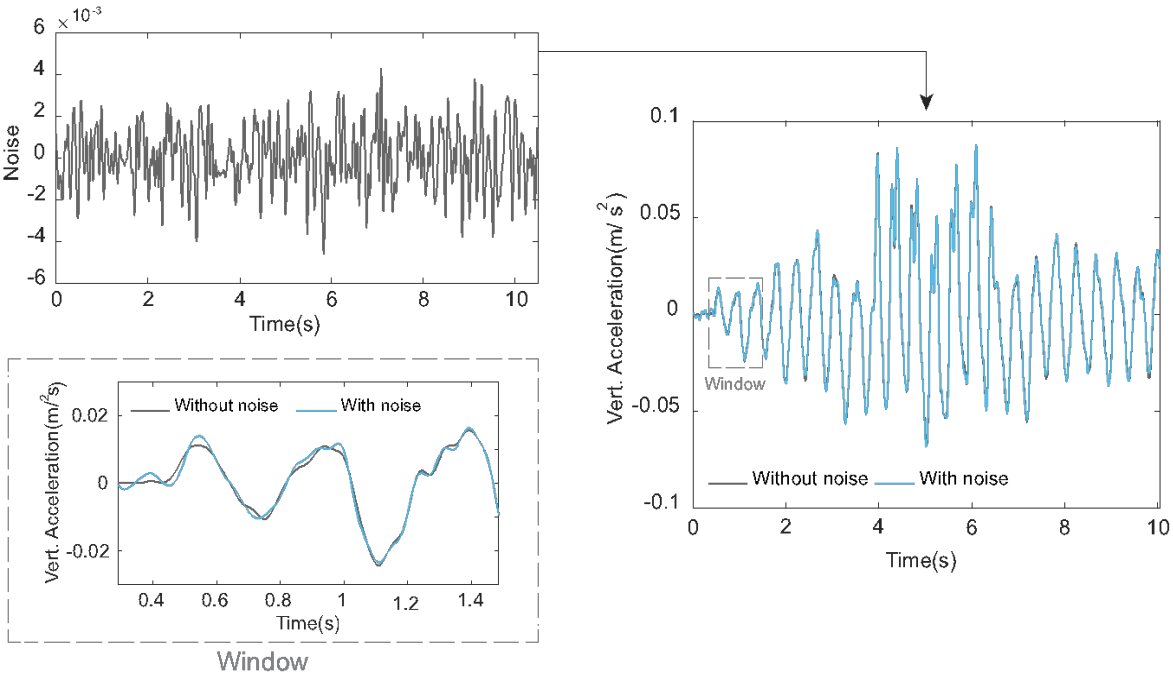

Figure 12. Noise distribution and vertical acceleration response of the bridge before and after being corrupted.

4.4 Numerical simulation

The simulation procedure applied to obtain responses describing damaged and undamaged structural conditions followed the procedure described in section 4.2, using the train loading configurations presented in Figure 7 at different speeds (according to Figure 10), as well as temperature data acquired on site (Figure 5) as input. The acceleration responses were then 'corrupted' with the noise distributions measured on site, as shown in the previous section.

The time-series illustrated from Figure 13 to Figure 15 are examples of simulated responses for baseline and damage conditions, acquired from the accelerometer located at the second mid-span of the concrete slab (Ac1). The variations associated with different train types, loading schemes, train speed and temperature are shown in Figure 13 and Figure 14. The first shows a clear distinction between the responses of the bridge for the passages of the AP train (Figure 13a) and the IC train (Figure 13b), evidencing the need of taking into account different train types for the development of damage detection methodologies. Conversely, the same figures allow observing that different loading schemes generate smaller changes in the dynamic responses. Temperature and train speed also influence the structural response imposed by trains crossing the bridge, as noted in Figure 14a and Figure 14b for AP train crossings.

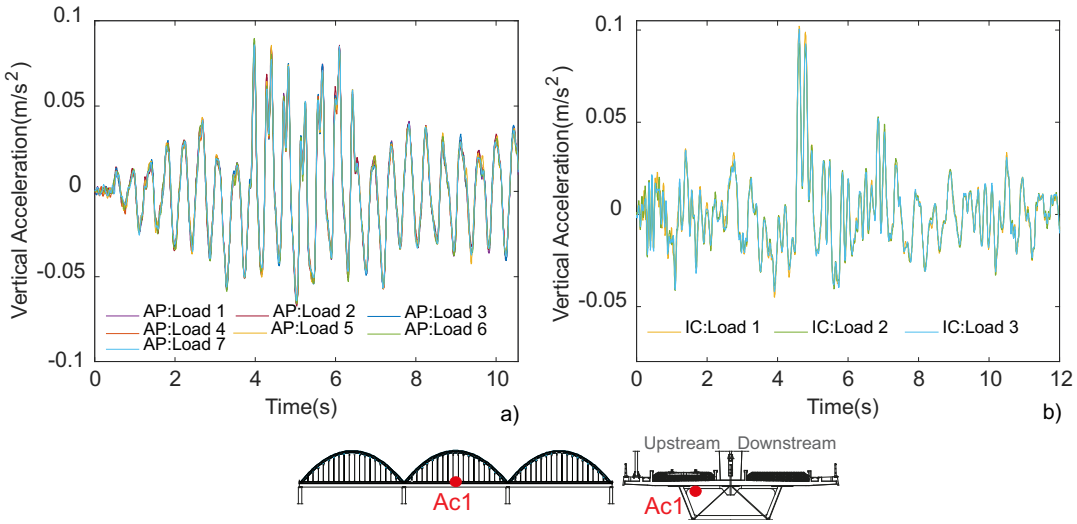

Figure 13. Baseline time-series simulations of sensor Ac1: a) using different loading schemes of the AP train at 220 km/h, b) using different loading schemes of the IC train at 190 km/h.

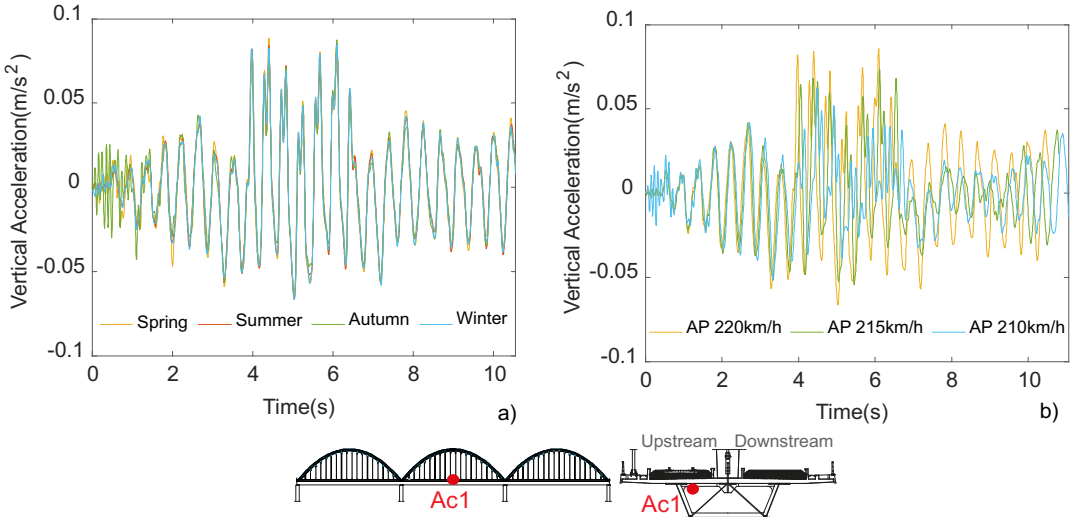

Figure 14. Baseline time-series simulations of sensor Ac1: a) using temperature measurements from different seasons, b) AP train crossing the bridge at different speeds.

As can be easily observed in Figure 15, the influence of the damage scenarios on the signal obtained for the crossing of trains appears to be much smaller than that observed in the changes in temperature, train type and train speed, even when regarding the sensors adjacent to the damages and the greater magnitudes considered (20% stiffness reductions). The high overlap of the time-series obtained from the baseline condition and the remaining ones show the small magnitude of the simulated damage scenarios, which can be straightforwardly considered as early-damage.

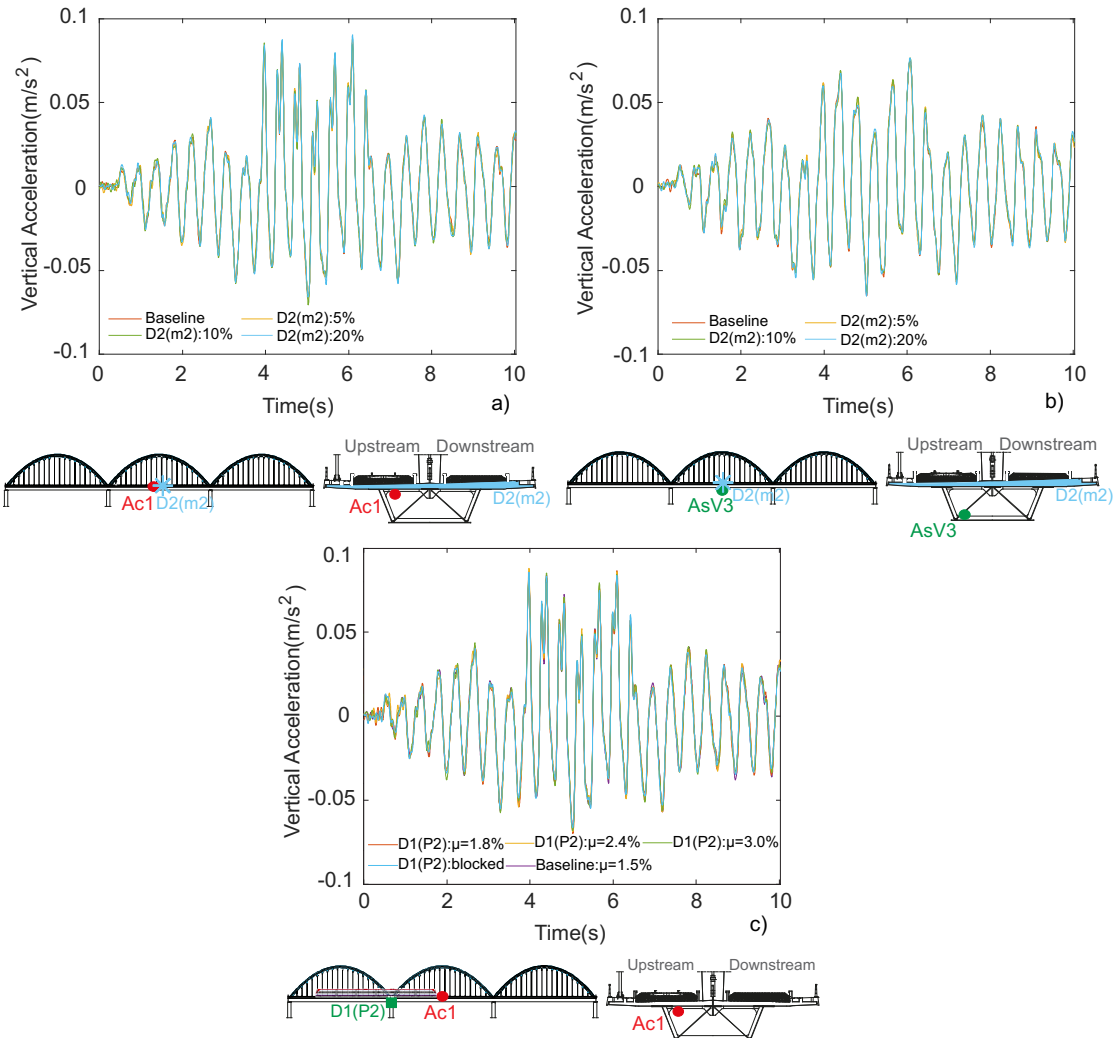

Figure 15. Time-series obtained for: a) stiffness reduction D2 and vertical acceleration Ac1, b) stiffness reduction D2 and vertical acceleration AsV3, c) friction increase D1(P2) and vertical acceleration Ac1.

5. Damage detection on the Sado Railway Bridge

5.1 Feature extraction using AR models

The first step of the methodology was to extract AR parameters as damage-sensitive features. The most suitable AR model order is initially unknown. This is a key issue, since a higher-order model may better match the data, but may not be generalized to other data sets. On the other hand, if one selects a low-order model, it will not necessarily capture the underlying response of the physical system [5]. Specific techniques to achieve this goal can be found in the literature, such as the well-known Bayesian Information Criterion (BIC) detailed in [55]. To find out an optimum order, one should examine a wide range of orders and choose a number with the minimum BIC value. With the purpose of establishing a common appropriate order, analyses of the BIC values were performed for twenty three independent AR (p) models of increasing order (p=1,2,…,60). Figure 16 shows the average BIC function resulting from analyses carried out on the 100 baseline time-series. As

observed, after the model order 30 the BIC values tend to stabilize indicating that higher orders do not provide relevant information for the construction of the model. Based on these assessments, for each structural condition and for each accelerometer, individual AR (30) models were implemented to fit the corresponding time-series and their parameters were used as damage-sensitive features. Hence, for each of the 100 baseline and 114 damaged structural conditions, and for each of the 23 accelerometers, m = 30 parameters were extracted, using the least squares technique, from time-series comprising 2112 measurements. The outcome was a three-dimensional matrix of *214-by-30-by-23*.

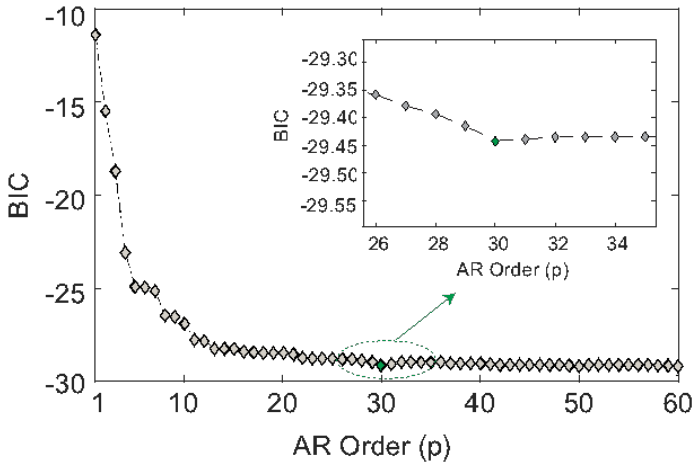

Figure 16. Average BIC plot for twenty-three independent AR (p) models of increasing order p using the 100 baseline time series.

AR parameters should be constant when estimated based on time-series data obtained from time-invariant systems. However, in the presence of environmental and operational variations, as well as damage, the parameters are expected to change [56], as shown in Figure 17, for each of the 100 simulations of the baseline condition and the 114 simulations of the damage condition, considering the measurements from one accelerometer located at the second mid-span of the concrete slab (Ac1). A comparison between the amplitude of the features in the different scenarios shows a greater variability of the AR parameters for EOVs than for damages.

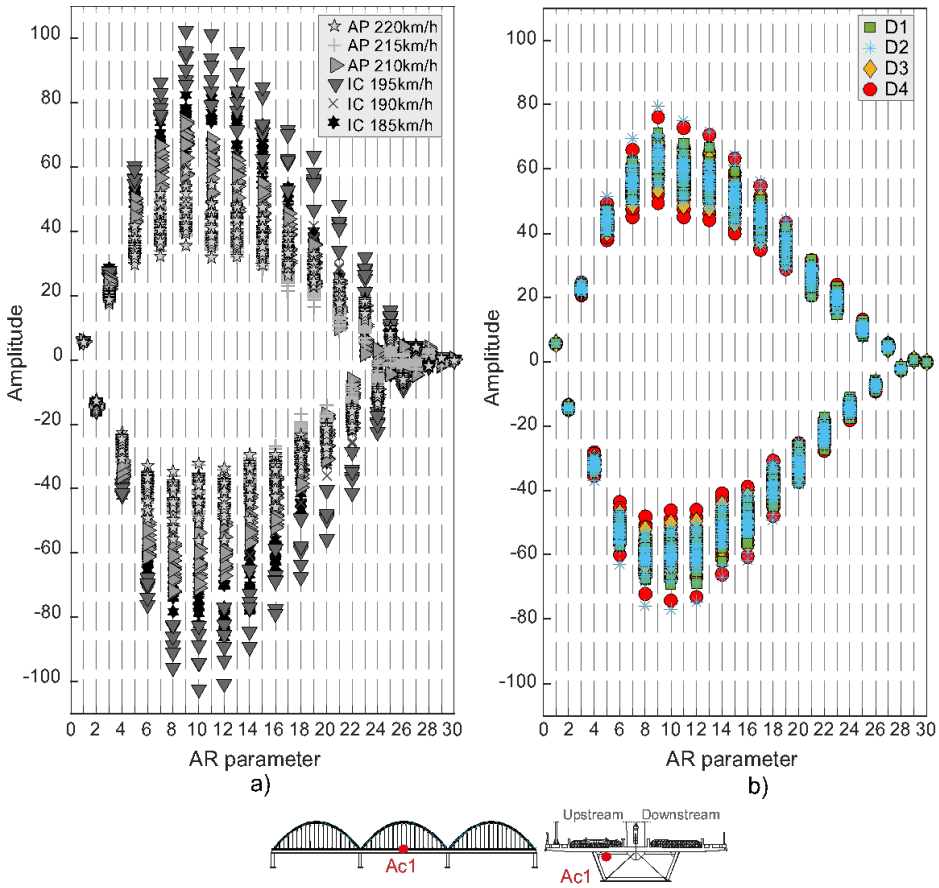

Figure 17. Features obtained from the acceleration responses in the mid-span section of the concrete slab (Ac1): a) for each of the 100 simulations of the baseline condition, b) for each of the 114 damage scenarios.

To illustrate the feature extraction procedure, all thirty AR parameters obtained for sensor Ac1 are represented by the box-and-whiskers plots in Figure 18b, of which five are shown in detail in Figure 18a. The features are divided according to the structural condition in two main groups: baseline (first 100 simulations) and damage (subsequent 114 simulations). A comparison between the values of the five parameters across all 214 scenarios allows concluding that each feature is describing distinct trends and inner relationships in the analysed data. The main changes in the amplitudes of the AR parameters are induced by the type and speed of the trains. In addition, for each speed value, the changes observed in the amplitude of the AR parameters are generated by changes in the structural temperature values (chosen for autumn, spring, summer or winter). The different loading schemes (the seven symbols in a row in the case of the AP and three symbols in a row in the case of the IC) considered for each train type and speed, and for each temperature, are the operational factors with the least impact on the parameter variability concerning the baseline simulations. In the plots shown in Figure 18a, for each damage location, the sequence of three or four symbols represent different levels of severity (low to high from left to right). Regardless of the type of damage (D1, D2, D3 or D4), its location (Figure 11) or severity (5%, 10% or 20%), the amplitude and distribution of the AR parameters vary significantly less when

compared to changes in operational and environmental actions, as observed both in the series of five parameters and in the box-and-whiskers plots.

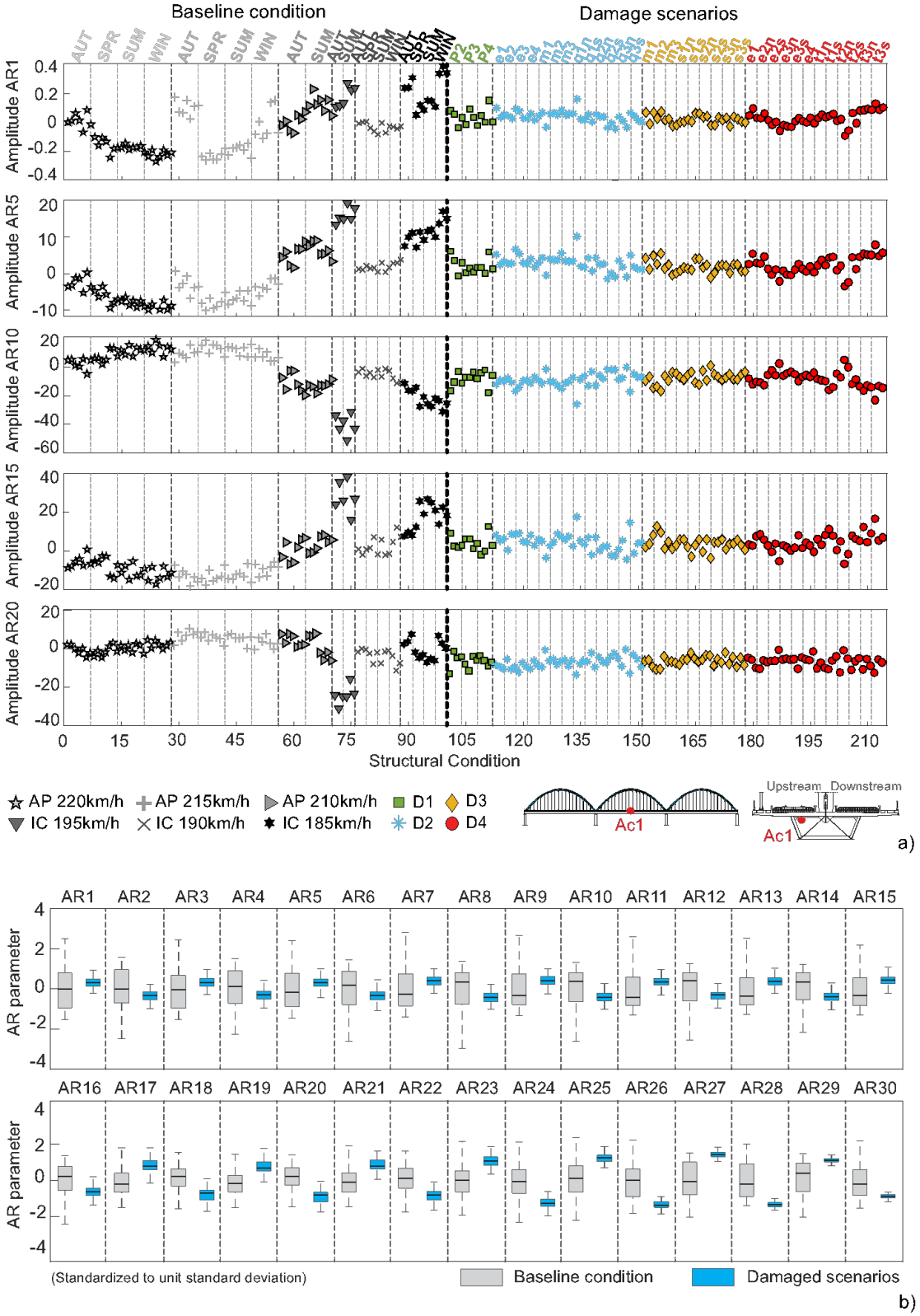

Figure 18. For all 214 structural conditions considering the responses of accelerometer Ac1: a) amplitude of five of the thirty AR parameters, b) box-and-whiskers plots representing the thirty AR parameters.

The importance of a disperse sensors network can be observed in Figure 19, where the features obtained from the accelerations of three sensors (Ac1, AL-P3 and AsₜT2) represent distinct distributions of AR parameters for each analysed state condition. This figure illustrates the AR parameters for two simulations of the baseline condition, where the varying operational factor is the train speed, as well as the features resulting from four damage scenarios, namely the full restrain of the bearing devices at pier P3 (D1), the 20% stiffness reduction in the second mid-span of the concrete slab (D2), the 20% stiffness reduction at the diaphragms, also in the second mid-span (D3), and the 20% stiffness reduction in the arch at one-third south of the central span (D4). The plots show that the amplitudes of the parameters for the Ac1 sensor are those with the most significant fluctuations, especially for the D2 damage condition, adjacent to this sensor. Regarding the AL-P3 sensor, the parameters with the greatest amplitude are those of the D1 damage scenario, which is also the closest to this sensor. On the other hand, the AsTₜ2 transversal accelerometer, located in the steel-box girder at one-third south of the central span, shows more sensitivity to parameters that result from a damage in the section closest to the arch (D4).

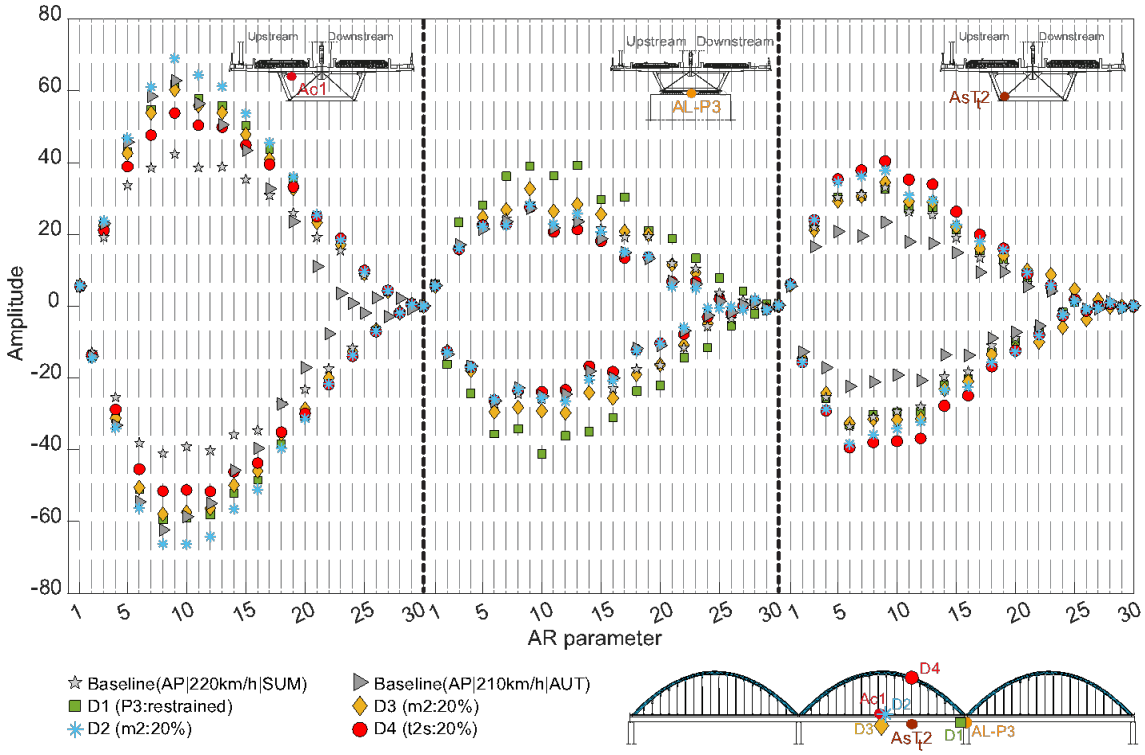

Figure 19. Features obtained from the acceleration responses measured by three sensors regarding two baseline and four damage structural conditions.

5.2 Feature modelling

5.2.1 Based on measured actions and structural responses

The analysis of the AR parameters shown in Figure 17 and Figure 18, as well as the time series presented in section 4.4, allow drawing some conclusions about the difficulty in distinguishing damage and undamaged scenarios, since changes in environmental and operational actions result in identical or greater changes in the parameters. As a result, it is necessary to adequately model these parameters to remove the changes generated by EOVs and highlight those generated by damage.

As previously stated, the modelling of the AR parameters was performed using MLR and latent variable methods. As mentioned in section 2.3, the regression models were fitted to the AR parameters to obtain, for each of the 214 train crossings, a new matrix of AR parameters of the same size (*30-by-23)*, which is assumed to be independent (as much as possible, given the error associated with modelling) from environmental and operational effects. Regressions were applied using the AR parameters as dependent, or predicted, variables (Y in Eq.(3)), and temperature measurements and train speeds as explanatory variables (X in Eq.(3)). Figure 20a shows the series of five parameters across the 214 scenarios obtained for the Ac1 accelerometer, after the application of the MLR. The direct comparison of these action-free AR parameters with those shown before the feature modelling (Figure 18a) allows observing that, in fact, the feature modelling enabled removing the effects generated by the type and speed of the train and by temperature, but not those generated by damage. As shown in Figure 20b, not only have the effects of the EOVs been mitigated, but an important improvement can be observed in the distinction between simulations of baseline and damage conditions in all thirty parameters.

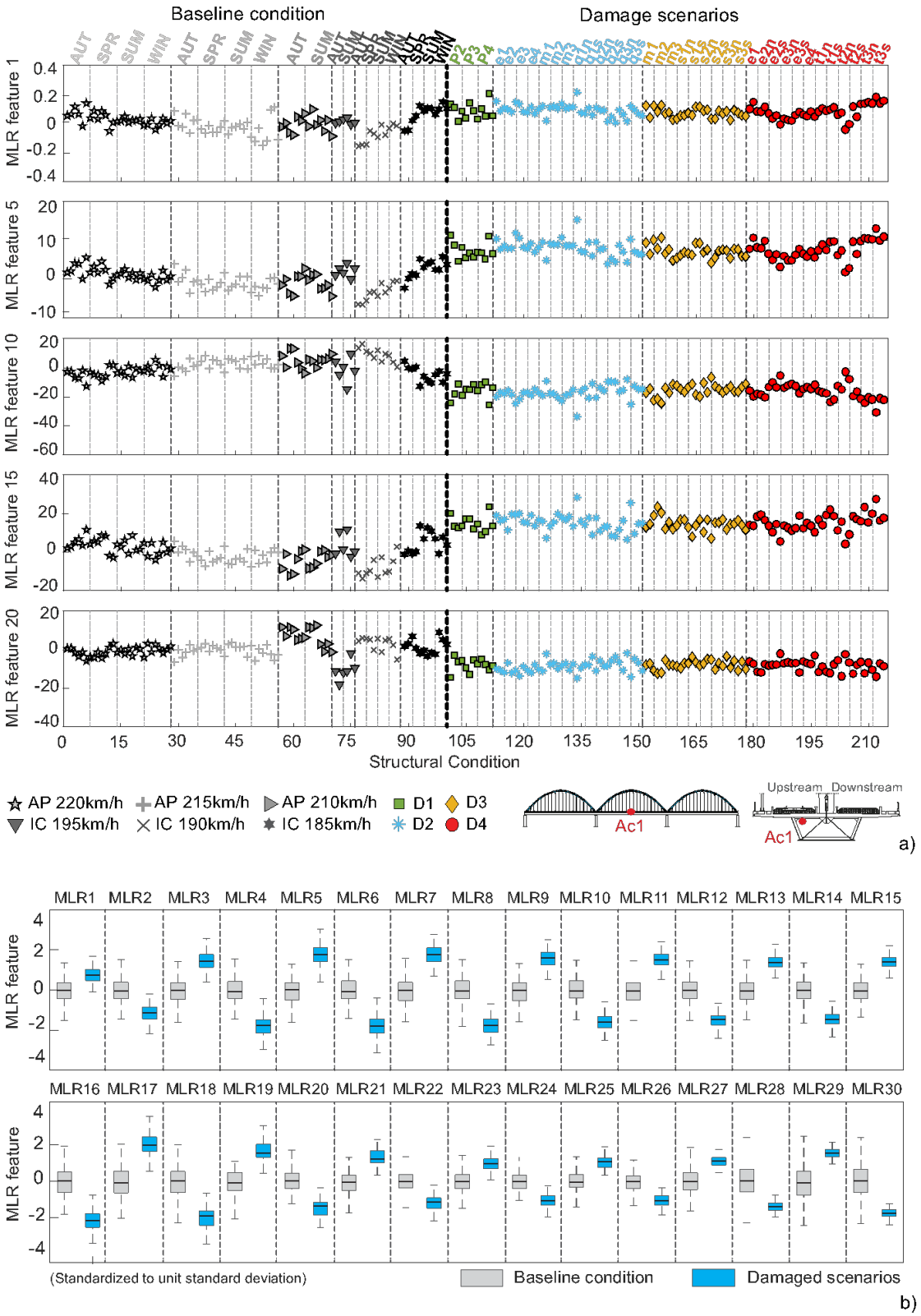

Figure 20. For all 214 structural conditions considering the responses of the Ac1 accelerometer: a) amplitude of five of the thirty MLR-based features, b) box-and-whiskers plots representing the thirty MLR-based features.

5.2.2 Based on structural response measurements alone

As an alternative to the MLR model, PCA-based modelling, as described in section 2.3, was applied to the AR parameters, and a *23-by-30* matrix with PCA-based features was obtained for each train crossing. The

important advantage of fitting a PCA model instead of an MLR model was the ability to remove the influence of temperature and train speed without having to measure them. Since the cumulative percentage of variance of the first principal component was greater than 80% for different structural conditions, this PC was the only one discarded during the modelling process (i.e. $p = 1$). Figure 21a shows the five AR parameters for the Ac1 accelerometer, obtained applying the PCA-based modelling.

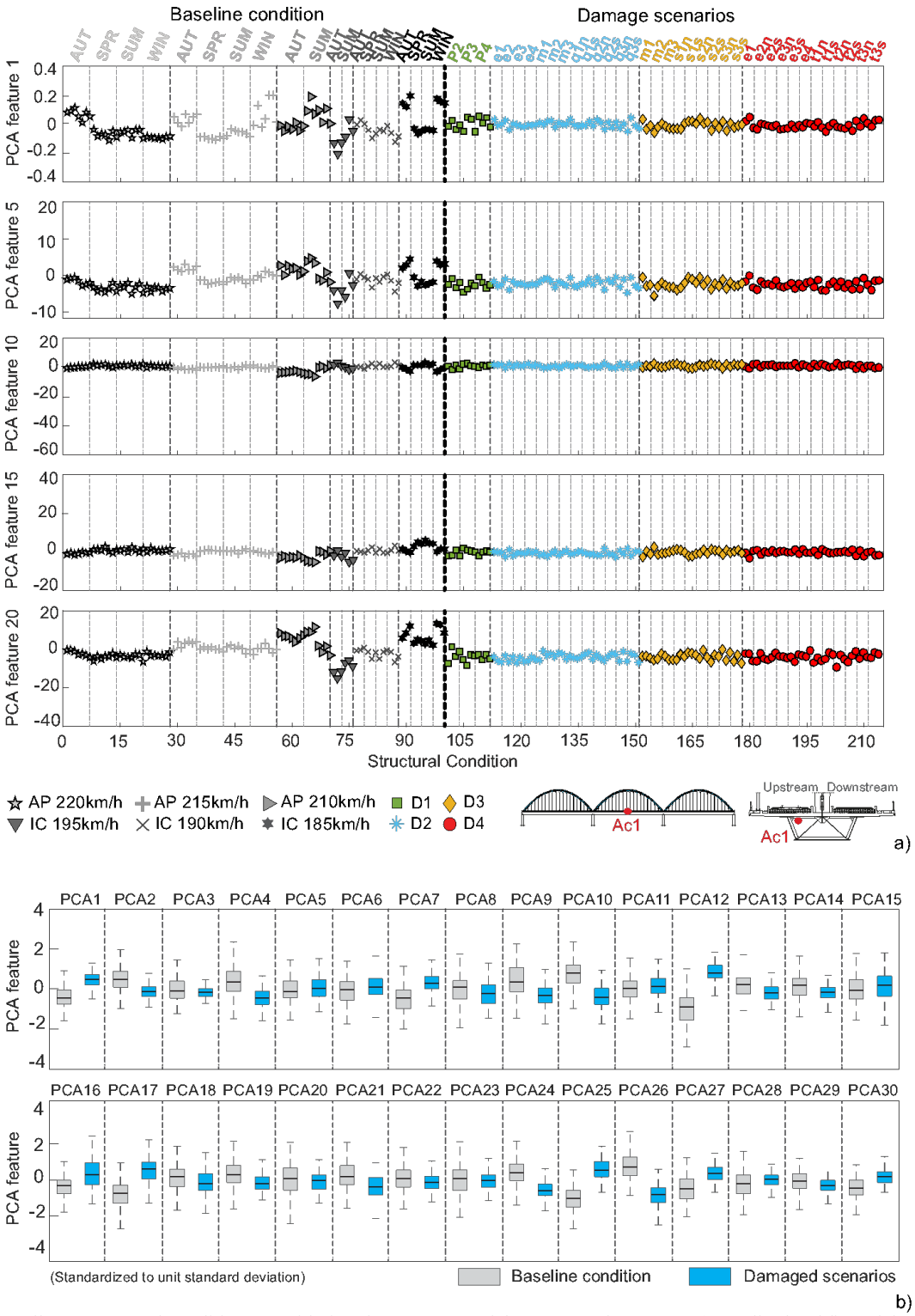

Figure 21. For all 214 structural conditions considering the responses of the Ac1 accelerometer: a) amplitude of five of the thirty PCA-based features, b) box-and-whiskers plots representing the thirty PCA-based features.

The comparison of these plots with those shown in Figure 18 also allows observing the suppression of the changes generated by environmental and operational actions even if a distinction between the baseline simulations and the damage scenarios is not as clear as that obtained when applying the MLR modelling (Figure 20). The same conclusions can be observed for all parameters represented by the box-and-whiskers plots in Figure 21b.

5.3 Data Fusion

5.3.1 Based on measured actions and structural responses

With the objective of merging all the AR parameters obtained for each acceleration sensor, the Mahalanobis distance was applied to the MLR-based features as shown in Figure 22 for the Ac1, AL-P3, and AsT_t2 sensors. The Mahalanobis distance allowed transforming, for each sensor and train crossing, the 30 AR parameters into one single feature (a distance in the feature space), which exhibits higher values for different structural conditions and null (or near-null) values for identical structural scenarios. The outcome of this procedure is a vector of *214-by-1,* of distances, one for each of the 23 sensors. The three plots in Figure 22 clearly show the difference in sensitivity for different sensors in each structural condition.

The accelerometer located at the second mid-span of the concrete slab (Ac1) exhibits an important global sensitivity to damage, since there is a distinction between the baseline simulations and the damage scenarios, but it is not efficient in distinguish the different types of simulated damages. Conversely, the longitudinal accelerometer on pier P3 (AL-P3) is more sensitive to damages on piers P3 and P4, with special emphasis on the damage related to the full restrain of the bearing devices on pier P3. The transversal accelerometer located in the steel box at one-third south of the central span (AsT_t2) also allows distinguishing between certain specific types and magnitudes of damage. Figure 23 allows observing the distribution obtained from each accelerometer (presented in Figure 5) and its high sensitivity to distinguish baseline and damage conditions.

In order to detect all damage scenarios, a data fusion of the MLR-based features of the 23 sensors located on the bridge was also implemented. It consists of applying the Mahalanobis distance to the 23 distances representing each sensor, thus resulting in a single DI *214-by-1* vector that represents all the data acquired through the 23 sensors. As a result, a clear distinction between simulations of the baseline condition and damage scenarios was achieved, as presented in Figure 24. Merging the information from all sensors, it is clear that the

damages related to the restrain of the bearing devices and the stiffness reduction of the concrete slab near the piers (e1 and e2) are those to which the sensing system appears to be more sensitive.

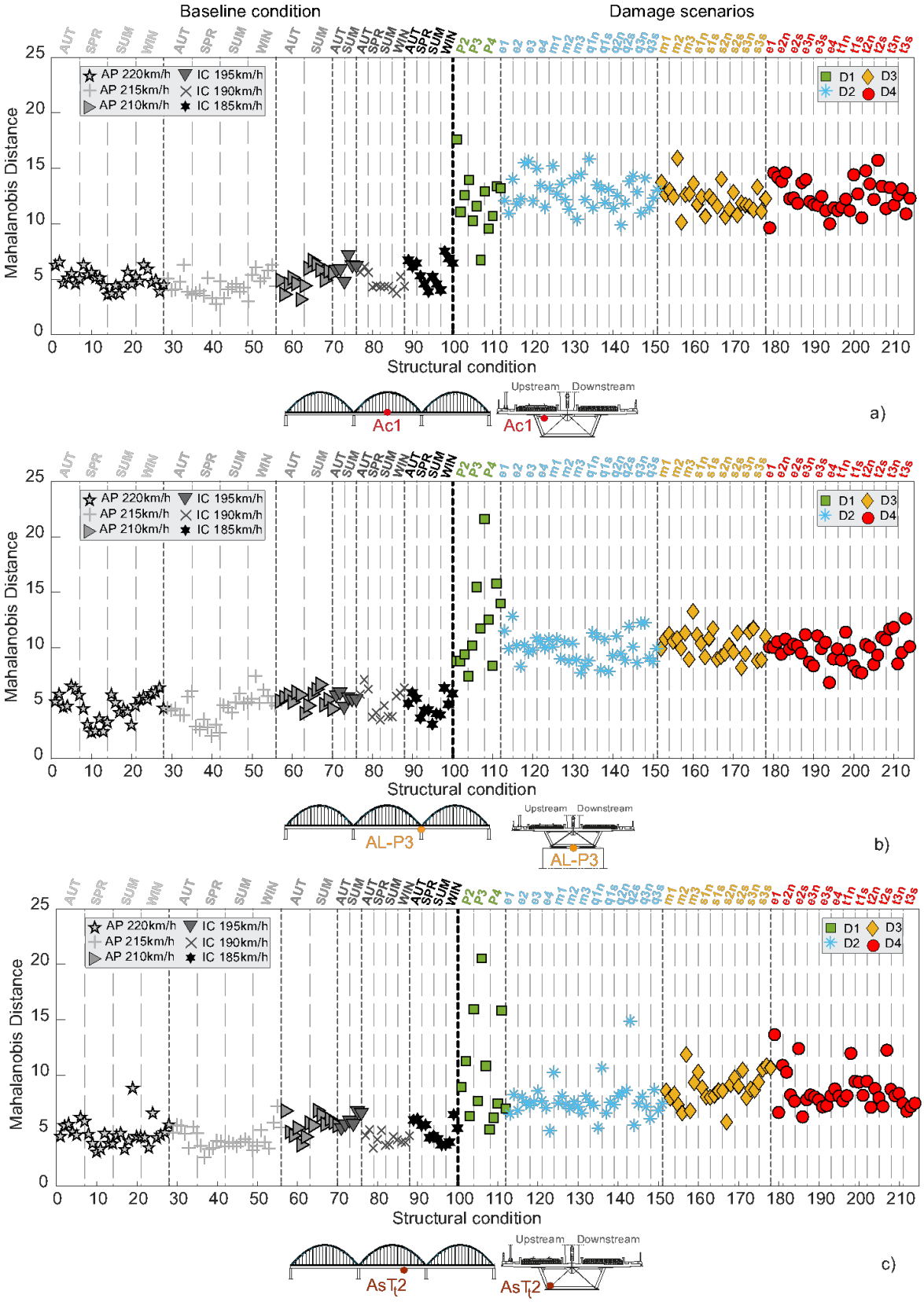

Figure 22. Mahalanobis distance of the MLR-based features for all 214 structural conditions, considering the responses from accelerometers: a) Ac1, b) AL-P3 and c) AsTt2.

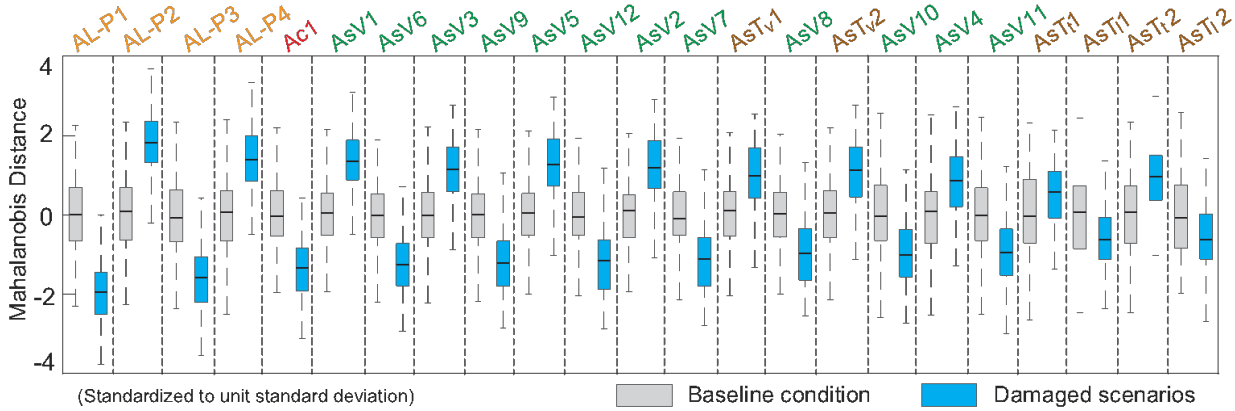

Figure 23. Box-and-whiskers plots representing, for each of the 23 sensors, the Mahalanobis distance of the MLR-based features for all 214 structural conditions.

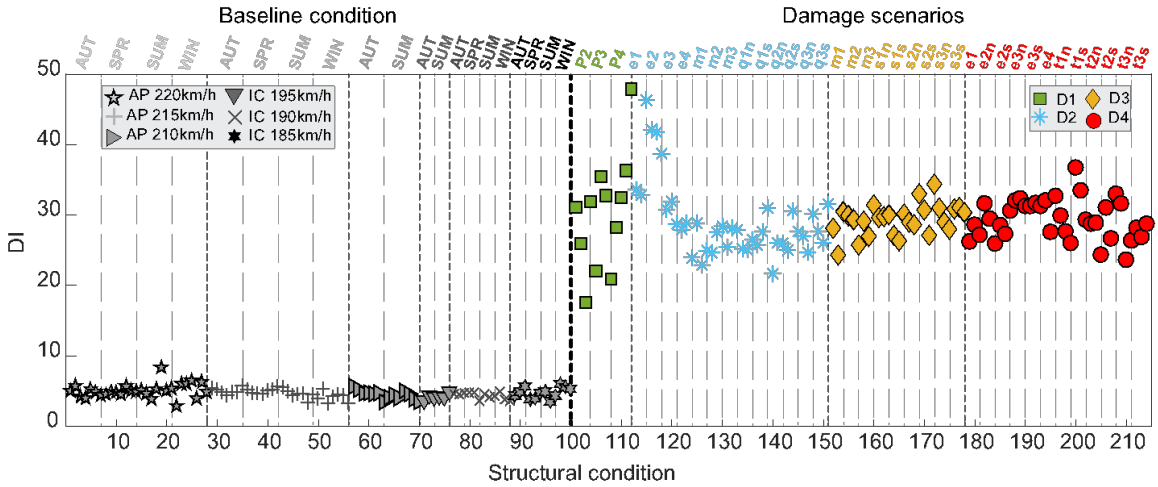

Figure 24. DI values obtained with MLR-based features for all 214 structural conditions considering the responses from all sensors.

5.3.2 Based on structural responses measurements alone

The procedure described in 5.3.1 for the MLR-based parameters is repeated herein for the PCA-based parameters. As with the results from the MLR, for each sensor, the Mahalanobis distance allowed transforming the 30 parameters from each train crossing into a single damage-sensitive feature. The features obtained for sensors A1, AL-P3, AsT$_l$2 are presented in Figure 25 and the box-and-whiskers plots representing the features extracted from each of the 23 accelerometers are shown in Figure 26, where most sensors reveal high sensitivity.

Using the PCA-based damage-sensitive features of all 23 sensors, the single series of *DI* values presented in Figure 27 was accomplished. Although the distances between the simulations of the baseline condition and the damage scenarios are not as great as those obtained from MLR-based parameters, it is still possible to clearly distinguish baseline from damage conditions, with the important advantage of not having to accurately measure temperature, nor identify the type and speed of the train. The combination of the information retained in this feature describing the data from all sensors also shows that the sensing system is more sensitive to damages on the bearing devices and on the concrete slab near the piers (e2 and e3).

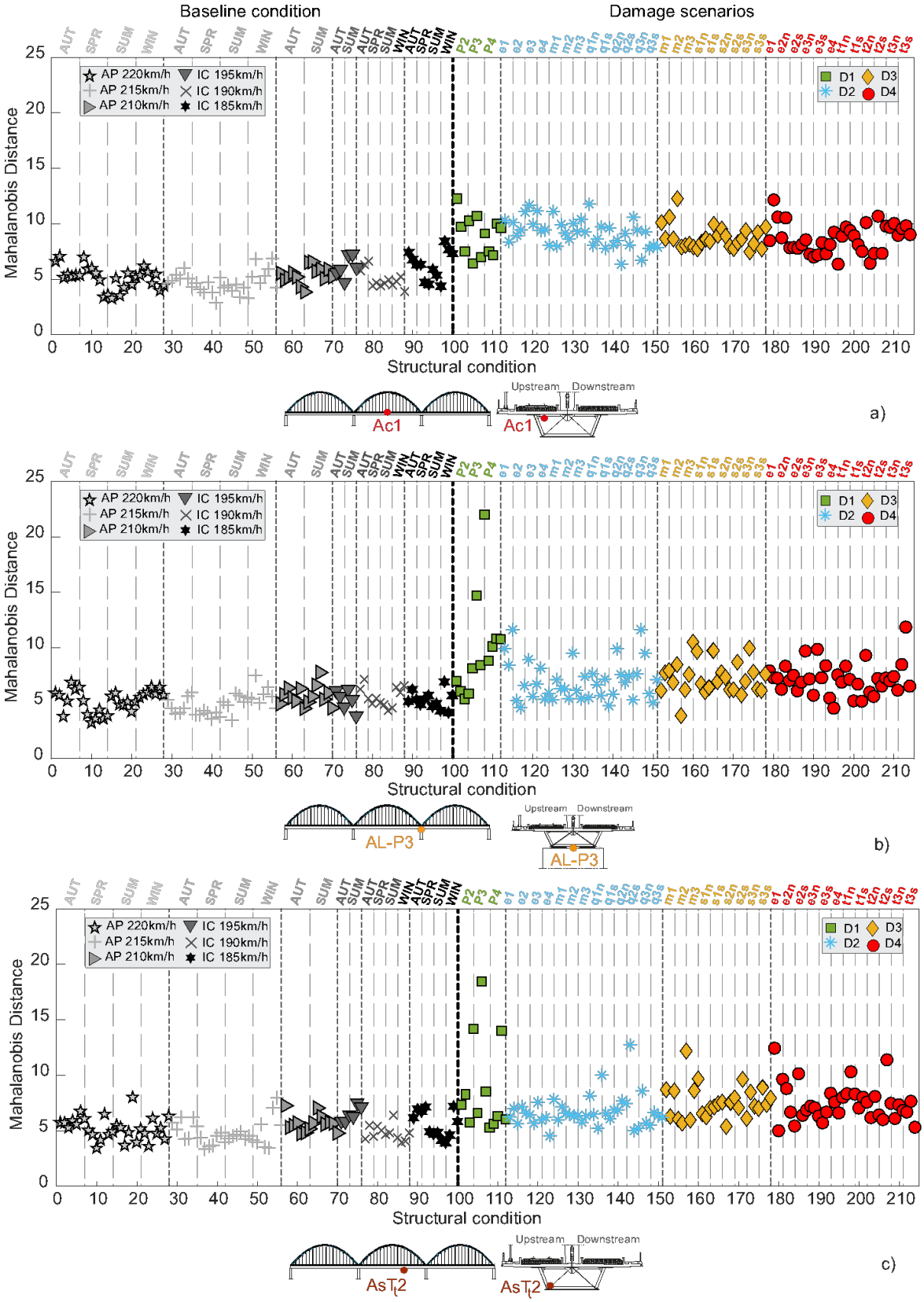

Figure 25. Mahalanobis distance of the PCA-based features for all 214 structural conditions, considering the responses from accelerometers: a) Ac1, b) AL-P3 and c) AsT_t2.

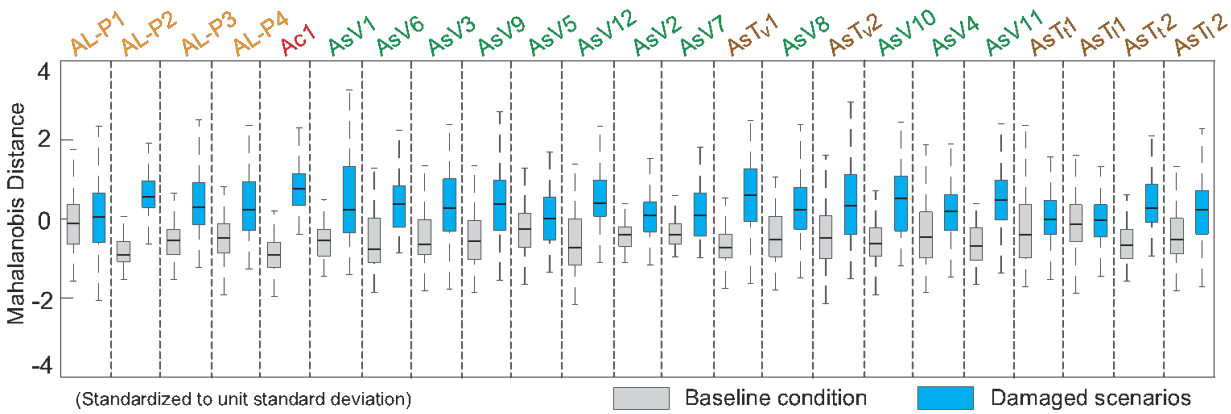

Figure 26. Box-and-whiskers plots representing, for each of the 23 sensors, the Mahalanobis distance of the PCA-based features for all 214 structural conditions.

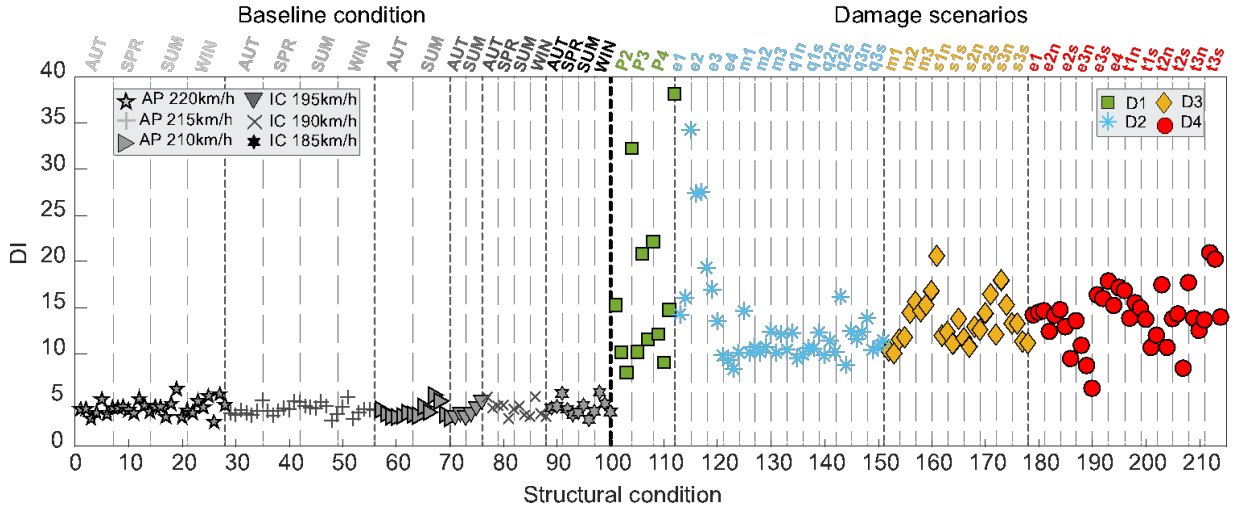

Figure 27. DI values obtained with PCA-based features for all 214 structural conditions considering the responses from all sensors.

5.4 Statistical-based automatic damage detection

The final step of the proposed methodology is the automatic detection of damages based on a CB computed using the Gaussian inverse cumulative distribution function. A significance level of 1% was defined, as it is commonly observed in several SHM works addressing damage identification [5, 15, 57]. Figure 28 allows observing the effectiveness of the methodology which, both for the features based on measured actions and structural responses (MLR-based), and for those based only on measured structural responses (PCA-based), allows distinguishing baseline from damage scenarios. The approach that uses an input-output method for feature modelling exhibits one (1%) Type I error (*false-positive*), regarding the crossing of an AP train at 220 km/h on a summer day with a loading scheme 5 (Figure 28a). The approach based on an output-only method (Figure 28b) exhibits one (0.88%) Type II error (*false-negative*) concerning a stiffness reduction in the arch of the second span in a section near pier P3 (e3n).

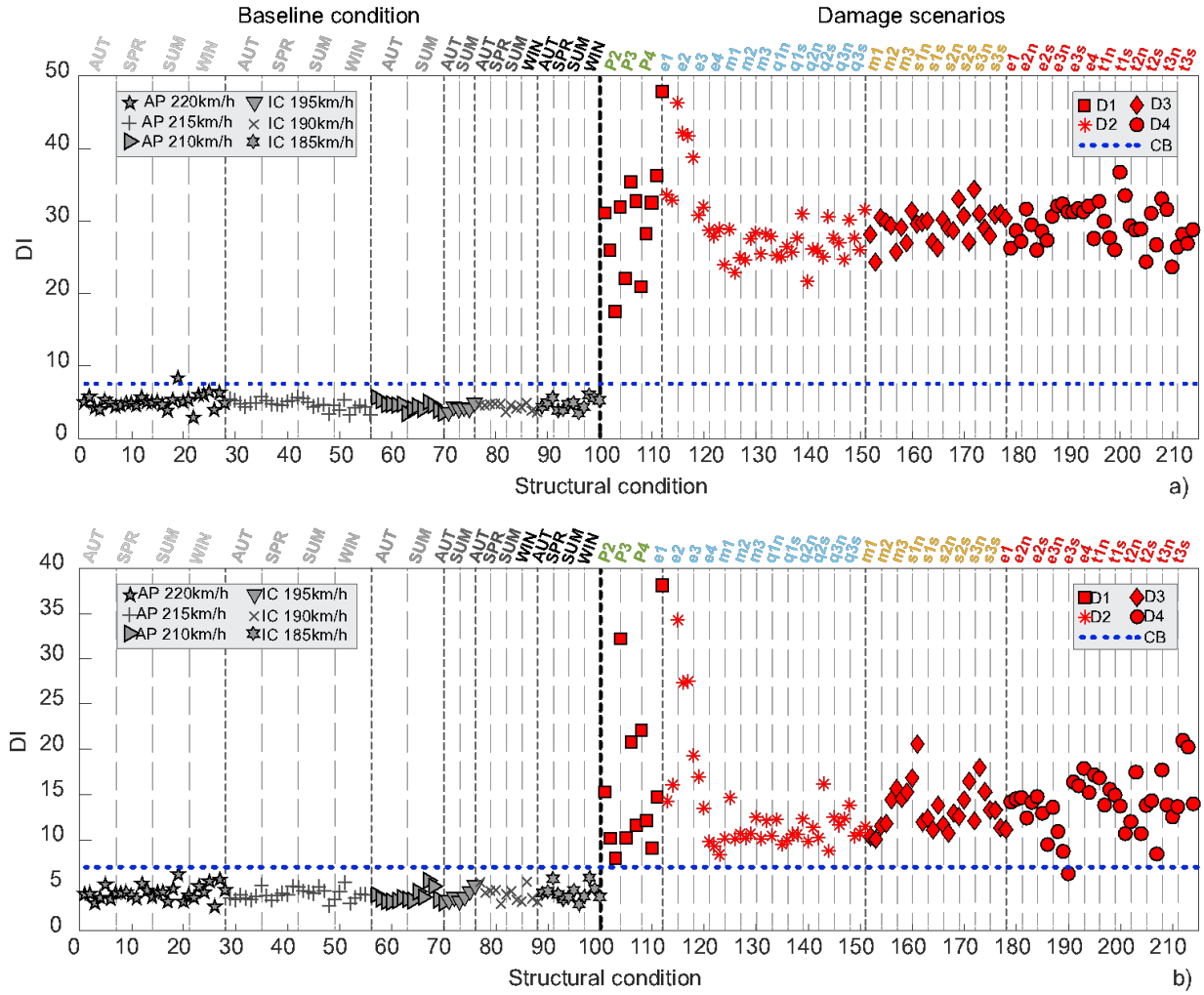

Figure 28. Automatic damage detection using *DI* values for all 214 structural conditions considering the responses from all sensors and a CB determined for a significance level of 1%: a) MLR-based features, b) PCA-based features.

6. Conclusions

This paper presents a novel SHM methodology for conducting unsupervised damage detection on railway bridges based on traffic-induced responses, applying time series analysis and multivariate statistics techniques. The developed methodology consists of fusing sets of acceleration measurements to improve sensitivity and combines: i) AR models, ii) PCA or MLR, iii) Mahalanobis distance and iv) outlier analysis.

Civil structures tend to be one-of-a-kind, large capital assets; as such, it is very difficult, if not impossible, to get access to damaged railway bridge data from the field. On top of that, even if there is damage, it will be very difficult to convince the owner to allow researcher access to it before maintenance actions are implemented, due to confidentiality and safety reasons. Therefore, the effectiveness of the proposed methodology was validated on a digital twin of a bowstring-arch railway bridge with a highly reliable description of the structure's stiffness, mass, and boundary conditions, as well as its response to environmental and operational actions. A comprehensive dataset of baseline and damaged scenarios was simulated using only

experimentally obtained actions as input, namely temperature, train loadings and speeds. To obtain the most similar and reliable reproduction of the real SHM data, each simulation was polluted with different noise signals acquired on site by each accelerometer, on different days, thus ensuring the most appropriate validation of the methodology developed herein. Damage severities of 5%, 10% and 20% of stiffness reductions in the concrete slab, diaphragm and arches were simulated, as well as friction increases in the movements of the bearing devices from a reference value of 1.5% to 1.8%, 2.4%, 3.0% and the full restrain of these elements.

The damage-sensitive features were extracted by fitting AR (30) models to the bridge accelerations induced by train crossings in different locations along the bridge. The study of the AR parameters obtained from different structural conditions, allowed drawing conclusions about the supremacy of the EOVs when compared with damage, proving the importance of feature modelling. On the other hand, the analysis of the AR parameters from different sensors showed that the information stored for each type of damage is different.

MLR and PCA were implemented to study the trade-off between modelling the features using input-output or output-only methods. Both approaches allowed for an undeniable reduction in the effects of EOVs, although the features obtained with MLR enable a clearer distinction between undamaged and damaged conditions.

To describe the variability present in the modelled features, a Mahalanobis distance was applied to the 30 features of each sensor. It was possible to verify that different sensors have greater or lesser sensitivity, depending on the location of the damage. To enhance sensitivity, the data fusion of the features extracted from all the sensors was implemented and a single damage indicator for each train crossing was defined and obtained. This step proved to be crucial to achieve the highest possible level of information fusion and to obtain a clear distinction between undamaged and damaged conditions for both approaches. Notwithstanding, the damage indicator values obtained with MLR-based features proved to be more sensitive than those obtained with PCA-based features.

In order to automatically detect the presence of damage, an outlier analysis was performed based on a CB computed for a significance level of 1%. The robustness and effectiveness of the proposed methodology was demonstrated by automatically detecting the damage scenarios as different from those belonging to the undamaged baseline. Using features modelled based on measured actions and structural responses (MLR-based), only one false-positive was exhibited (1% incidence), while with features modelled based on structural response measurements alone (PCA-based), only one false-negative was obtained (0.88% incidence). The

results showed that even in an SHM system without the ability of measuring environmental and operational effects, it is possible to successfully detect different types of damage using the bridge's responses to train crossings. In short, the proposed methodology, which considers a PCA for feature modelling, in addition to being efficient, has the advantages of minimizing the number of sensors that need to be installed and, consequently, the cost of the SHM system, as well as allowing for a more automatic and straightforward implementation.

The study of multiple damage scenarios, a sensitivity/robustness analysis to optimize the number of sensors in the SHM system, as well as, the efficiency of this methodology in case of sensor malfunctions, will be included in the scope of future works.

Acknowledgements

This work was financially supported by the Portuguese Foundation for Science and Technology (FCT) through the PhD scholarship SFRH/BD/93201/2013. The authors would like to acknowledge the support of the Portuguese Road and Railway Infrastructure Manager (Infraestruturas de Portugal, I.P), the Portuguese National Laboratory for Civil Engineering (LNEC), the SAFESUSPENSE project - POCI-01-0145-FEDER-031054 (funded by COMPETE2020, POR Lisboa and FCT) and the Base Funding - UIDB/04708/2020 of the CONSTRUCT - Instituto de I&D em Estruturas e Construções - financed by national funds through the FCT/MCTES (PIDDAC).

References

1. Carey CH, O'Brien EJ, Keenahan J. Investigating the Use of Moving Force Identification Theory in Bridge Damage Detection. *Key Engineering Materials* 2013; **569**–**570**: 215–222. DOI: 10.4028/www.scientific.net/KEM.569-570.215.
2. Cantero D, González A. Bridge Damage Detection Using Weigh-in-Motion Technology. *Journal of Bridge Engineering* 2015; **20**(5): 04014078–1 to 04014078–10. DOI: 10.1061/(ASCE)BE.1943-5592.0000674.
3. Huang Q, Gardoni P, Hurlebaus S. A probabilistic damage detection approach using vibration-based nondestructive testing. *Structural Safety* 2012; **38**: 11–21. DOI: 10.1016/j.strusafe.2012.01.004.
4. Glaser SD, Tolman A. Sense of Sensing: From Data to Informed Decisions for the Built Environment. *Journal of Infrastructure Systems* 2008; **14**(1): 4–14. DOI: 10.1061/(ASCE)1076-0342(2008)14:1(4).
5. Farrar CR, Worden K. *Structural Health Monitoring: a machine learning perspective*. Wiley; 2013.
6. Sohn H, Czarnecki CRFFMH, Shunk DD, Stinemates DW, Nadler BR, Czarnecki JJ. *A Review of Structural Health Monitoring Literature : 1996 – 2001*. Los Alamos (USA): 2004.
7. Posenato D, Lanata F, Inaudi D, Smith IFC. Model-free data interpretation for continuous monitoring of complex structures. *Advanced Engineering Informatics 22* 2008; **22**: 135–144. DOI: 10.1016/j.aei.2007.02.002.
8. Rytter A. *Vibrational Based Inspection of Civil Engineering Structures*. Aalborg: Dept. of Building Technology and Structural Engineering, Aalborg University: 1993.
9. Worden K, Dulieu-Barton JM. An Overview of Intelligent Fault Detection in Systems and Structures. *International Journal of Structural Health Monitoring* 2004; **3**(1): 85–98.
10. Farrar C, Sohn H, Worden K. Data Normalization : A Key For Structural Health Monitoring. *Technical Report, Los Alamos National Laboratory* 2001; **836**(LA-UR-01-4).
11. Yan A, Kerschen G, Boe P De, Golinval J. Structural damage diagnosis under varying environmental conditions — Part I : A linear analysis. *Mechanical Systems and Signal Processing* 2005; **19**: 847–864. DOI: 10.1016/j.ymssp.2004.12.002.
12. Alvandi A, Cremona C. Assessment of vibration-based damage identification techniques. *Journal of Sound and Vibration* 2006; **292**: 179–202. DOI: 10.1016/j.jsv.2005.07.036.
13. Alves V, Meixedo A, Ribeiro D, Calçada R, Cury A. Evaluation of the performance of different damage indicators in railway bridges. *Procedia Engineering* 2015; **114**: 746–753. DOI: 10.1016/j.proeng.2015.08.020.

14. Meixedo A, Alves V, Ribeiro D, Cury A, Calçada R. Damage identification of a railway bridge based on genetic algorithms. *Maintenance, Monitoring, Safety, Risk and Resilience of Bridges and Bridge Networks - Proceedings of the 8th International Conference on Bridge Maintenance, Safety and Management, IABMAS 2016*, Foz Do Iguaçu; Brazil: 2016.

15. Santos JP, Crémona C, Calado L, Silveira P, Orcesi AD. On-line unsupervised detection of early damage. *Structural Control and Health Monitoring* 2015. DOI: 10.1002/stc.

16. Santos JP, Crémona C, Orcesi AD, Silveira P. Multivariate statistical analysis for early damage detection. *Engineering Structures* 2013; **56**: 273–285. DOI: 10.1016/j.engstruct.2013.05.022.

17. Cury A, Cremona C. Assignment of structural behaviours in long-term monitoring : Application to a strengthened railway bridge. *Structural Health Monitoring* 2012; **11**(4): 422–441. DOI: 10.1177/1475921711434858.

18. Posenato D, Kripakaran P, Smith IFC. Methodologies for model-free data interpretation of civil engineering structures. *Computers & Structures* 2010; **88(7-8)**: 467–482. DOI: 10.1016/j.compstruc.2010.01.001.

19. Figueiredo E, Park G, Farrar CR, Worden K, Figueiras J. Machine learning algorithms for damage detection under operational and environmental variability. *Structural Health Monitoring* 2010; **10(6)**: 559–572. DOI: 10.1177/1475921710388971.

20. Datteo A, Busca G, Quattromani G, Cigada A. On the use of AR models for SHM: A global sensitivity and uncertainty analysis framework. *Reliability Engineering and System Safety* 2018; **170**: 99–115. DOI: 10.1016/j.ress.2017.10.017.

21. Lautour OR De, Omenzetter P. Damage classification and estimation in experimental structures using time series analysis and pattern recognition. *Mechanical Systems and Signal Processing* 2010; **24**: 1556–1569. DOI: 10.1016/j.ymssp.2009.12.008.

22. Azim R, Gül M. Damage detection of steel girder railway bridges utilizing operational vibration response. *Structural Control and Health Monitoring* 2019(August): 1–15. DOI: 10.1002/stc.2447.

23. Entezami A, Shariatmadar H. An unsupervised learning approach by novel damage indices in structural health monitoring for damage localization and quantification. *Structural Health Monitoring* 2017; **I**–**21**. DOI: 10.1177/1475921717693572.

24. Mujica LE, Gharibnezhad F, Rodellar J, Todd M. Considering temperature effect on robust principal component analysis orthogonal distance as a damage detector. *Structural Health Monitoring* 2020; **19**(3): 781–795. DOI: 10.1177/1475921719861908.

25. Cavadas F, Smith IFC, Figueiras J. Damage detection using data-driven methods applied to moving-load responses. *Mechanical Systems and Signal Processing* 2013; **39**(1–2): 409–425. DOI: 10.1016/j.ymssp.2013.02.019.

26. Peeters B, Roeck G de. One-year monitoring of the Z24 Bridge environmental effects versus damage events. *Earthquake Engineering and Structure Dynamics* 2001; **30**(2): 149–171.

27. Haynes C, Todd M. Enhanced damage localization for complex structures through statistical modeling and sensor fusion. *Mechanical Systems and Signal Processing* 2015; **54**–**55**: 195–209. DOI: 10.1016/j.ymssp.2014.08.015.

28. Hu W hua, Moutinho C, Caetano E, Magalhães F, Cunha Á. Continuous dynamic monitoring of a lively footbridge for serviceability assessment and damage detection. *Mechanical Systems and Signal Processing* 2012. DOI: 10.1016/j.ymssp.2012.05.012.

29. Farrar CR, Worden K. An introduction to structural health monitoring. *Philosophical Transactions of the Royal Society A: Mathematical, Physical and Engineering Sciences* 2007; **365**(1851): 303–315. DOI: 10.1098/rsta.2006.1928.

30. Gonzalez I, Karoumi R. BWIM aided damage detection in bridges using machine learning. *Journal of Civil Structural Health Monitoring* 2015; **5**(5): 715–725. DOI: 10.1007/s13349-015-0137-4.

31. Neves AC, González I, Leander J, Karoumi R. Structural health monitoring of bridges : a model-free ANN-based approach to damage detection. *Journal of Civil Structural Health Monitoring* 2017(7): 689–702. DOI: 10.1007/s13349-017-0252-5.

32. Nie Z, Lin J, Li J, Hao H, Ma H. Bridge condition monitoring under moving loads using two sensor measurements. *Structural Health Monitoring* 2019: 1–21. DOI: 10.1177/1475921719868930.

33. Entezami A, Shariatmadar H. Data-driven damage diagnosis under environmental and operational variability by novel statistical pattern recognition methods. *Structural Health Monitoring* 2018; **I**–**28**. DOI: 10.1177/1475921718800306.

34. Kantz H, Schreiber T. *Nonlinear time-series analysis*. Cambridge: Cambridge University Press; 2003.

35. Box G, Jenkins G. *Time Series Analysis: Forecasting and Control*. Englewood Cliffs, NJ: Prentice Hall; 1976.

36. Johnson RA, Wichern DW. *Applied Multivariate Statistical Analysis*. 6th ed. Harlow: Pearson; 2013.

37. Hu WH, Moutinho C, Caetano E, Magalhes F, Cunha L. Continuous dynamic monitoring of a lively footbridge for serviceability assessment and damage detection. *Mechanical Systems and Signal Processing* 2012; **33**: 38–55. DOI: 10.1016/j.ymssp.2012.05.012.

38. Magalhães F, Cunha A, Caetano E. Vibration based structural health monitoring of an arch bridge : From automated OMA to damage detection. *Mechanical Systems and Signal Processing* 2012; **28**: 212–228. DOI: 10.1016/j.ymssp.2011.06.011.

39. Härdle WK, Simar L. *Applied Multivariate Statistical Analysis*. 4th ed. Springer; 2015.

40. Jolliffe IT. *Principal Component Analysis*. 2nd ed. New York: Springer; 2002.

41. Worden K, Sohn H, Farrar CR. Novelty detection in a changing environment: regression and interpolation approaches. *Journal of Sound and Vibration* 2002; **258**(4): 741–761. DOI: 10.1006/jsvi.2002.5148.

42. Yeager M, Gregory B, Key C, Todd M. On using robust Mahalanobis distance estimations for feature discrimination in a damage detection scenario. *Structural Health Monitoring* 2019; **18**(1): 245–253. DOI: 10.1177/1475921717748878.

43. REFER. Variante de Alcácer 2010.

44. GRID, GREISH, BEG, FERBRITAS. Variante de Alcácer: Projecto de Execução do travessamento do Rio Sado 2006.

45. ANSYS. Academic Research. Release 17.1 2016.

46. Albuquerque C, Silva ALL, Jesus AMP De, Calçada R. An efficient methodology for fatigue damage assessment of bridge details using modal superposition of stress intensity factors. *International Journal of Fatigue* 2015; **81**: 61–77. DOI: 10.1016/j.ijfatigue.2015.07.002.

47. Min X, Santos L. *Ensaios dinâmicos da ponte ferroviária sobre o rio sado na variante de alcácer*. Lisboa [Portuguese]: 2011.

48. Ribeiro D, Calçada R, Delgado R, Brehm M, Zabel V. Finite element model updating of a bowstring-arch railway bridge based on experimental modal parameters. *Engineering Structures* 2012; **40**: 413–435. DOI: 10.1016/j.engstruct.2012.03.013.

49. Meixedo A, Ribeiro D, Santos J, Calçada R, Todd M. Progressive numerical model validation of a bowstring-arch railway bridge based on a structural health monitoring system. *Journal of Civil Structural Health Monitoring* 2021. DOI: 10.1007/s13349-020-00461-w.

50. Pimentel R, Barbosa M, Costa N, Ribeiro D, Ferreira L, Araújo F, *et al.* Hybrid Fiber-Optic / Electrical Measurement System for Characterization of Railway Traffic and Its Effects on a Short Span Bridge. *IEEE SENSORS JOURNAL* 2008; **8**(7): 1243–1249. DOI: 10.1109/JSEN.2008.926519.

51. Santos J. Smart Structural Health Monitoring Techniques for Novelty Identification in Civil Engineering Structures. PhD Thesis. Instituto Superior Técnico - University of Lisbon, 2014.

52. Wardhana K, Hadipriono FC, Asce F. Analysis of Recent Bridge Failures in the United States. *Journal of Performance of Constructed Facilities* 2003; **17**(3): 144–150.

53. Akesson B. *Understanding Bridge Collapses*. 1st ed. London, UK: Taylor & Francis; 2008.

54. Mohiuddin A. Khan. *Bridge and Highway. Structure Rehabilitation and Repair*. 1st ed. New York, USA: McGraw-Hill; 2010.

55. Bisgaard S, Kulahci M. *Time series analysis and forecasting by example*. Hoboken, NJ: John Wiley & Sons; 2011.

56. Figueiredo E, Figueiras J, Park G, Farrar CR, Worden K. Influence of the autoregressive model order on damage detection. *Computer-Aided Civil and Infrastructure Engineering* 2011; **26**(3): 225–238. DOI: 10.1111/j.1467-8667.2010.00685.x.

57. Tomé E, Pimentel M, Figueiras J. Damage detection under environmental and operational effects using cointegration analysis – Application to experimental data from a cable-stayed bridge. *Mechanical Systems and Signal Processing* 2020; **135**: 4–8.